ANALYSIS OF CANTILEVERS FOR HIGH-SPEED ATOMIC FORCE MICROSCOPY

A Thesis Submitted to
the Graduate School of Engineering and Sciences of
İzmir Institute of Technology
in Partial Fulfilment of the Requirements for the Degree of

MASTER OF SCIENCE

in Electronics and Communication Engineering

by
Harpreet Singh BRAR

July, 2018
İZMİR

We approve the thesis of **Harpreet Singh BRAR**

Examining Committee Members:

Assoc. Prof. Dr. Müjdat BALANTEKİN

Department of Electrical and Electronics Engineering
Izmir Institute of Technology

Assist. Prof. Dr. Barbaros ÖZDEMİREL
Department of Electrical and Electronics Engineering
Izmir Institute of Technology

Assist. Prof. Dr. Gökhan UTLU

Department of Physics, Ege University

09/07/2018

Assoc. Prof. Dr. Müjdat BALANTEKİN
Supervisor, Department of Electrical and Electronics Engineering
Izmir Institute of Technology

Prof. Dr. Enver TATLICIOĞLU

Head of Department of Electrical
and Electronics Engineering

Prof. Dr. Aysun SOFUOĞLU

Dean of the Graduate School of
Engineering and Sciences

ACKNOWLEDGMENTS

I would like to express my sincere gratitude to my advisor and mentor Assoc. Prof. Dr. Müjdat BALANTEKİN, who helped me in finding the topic of my thesis and completing my research with enthusiasm and innovation. No words of gratitude can suffice in thanking him for the time he took to discuss the vital parts of my work.

I would also like to show my indebtedness to my parents Manjit Kaur BRAR and Ikattar Singh BRAR for their unwavering faith and their enduring prayers. My sister Kamalpreet Kaur BRAR deserves a share of my gratitude as well. I also feel compelled to thank Dr. Muhammad JAWAD and Dr. Muzammil KHURSHID for their continuous support and encouraging attitude which kept my spirits high throughout the Master's program.

Also, I would like to express my recognition to all my colleagues and friends for their moral support. In the end, I cannot miss the occasion to thank the "Presidency for Turks Abroad and Related Communities (YTB)" for their financial support in accomplishing my Master's degree.

ABSTRACT

ANALYSIS OF CANTILEVERS FOR HIGH-SPEED ATOMIC FORCE MICROSCOPY

In life sciences, High-Speed Atomic Force Microscopy (HS-AFM) is now widely accepted as a dynamic event visualizer for numerous biological samples such as live cells, membrane lipids, ATP-proteins, enzymatic reactions, DNA-protein interactions, etc. HS-AFM's unique ability to observe surface topography of the samples with height data and with a resolution of up-to a single atom makes it a prominent tool in Nano measurements.

HS-AFM Imaging technique's speed and response is limited by various factors including cantilever probes, operating environment, scanning techniques etc. Cantilevers are indispensable and integral part of HS-AFM Systems, thereby necessitating their own critical evaluations. Therefore, evaluation of various parameters like resonance frequency, stiffness and *Q*-factor of cantilevers is an active area of research.

The simulated research work mimics the experimental conditions of HS-AFM operation in air and liquid environment. The damping mechanisms such as viscous and acoustic damping of the medium, squeeze film damping, and damping due to viscoelasticity of the material are included in the finite element simulations. High frequency soft cantilevers suitable for HS-AFM with the stiffness of ~1 N/m and with the first flexural eigenmode resonance frequency of ~1.5 MHz (in liquid) and ~5 MHz (in air) are studied. Numerous small rectangular and modified cantilevers of Silicon and Polymer (SU-8) materials with the length of ~5 to 10 μm, width of ~1 to 2.5 μm and thickness of ~0.1 to 0.6 μm are analyzed. Our aim in this research is to identify appropriate cantilever geometries and materials for HS-AFM applications.

ÖZET

YÜKSEK HIZLI ATOMİK KUVVET MİKROSKOBU İÇİN KONSOLLARIN ANALİZİ

Yaşam bilimlerinde, Yüksek-Hızlı Atomik Kuvvet Mikroskobu (YH-AKM) canlı hücreler, membran lipidleri, ATP-proteinleri, enzimatik reaksiyonlar, DNA-protein etkileşimleri, vs., gibi birçok biyolojik örneğin dinamik olay görüntüleyicisi olarak günümüzde yaygın bir şekilde kabul edilmektedir. YH-AKM'nin örneklerin yüzey topografyasını yükseklik bilgisiyle ve tek atom çözünürlüğüne kadar eşsiz gözlemleyebilme yetisi onu Nano ölçümlerde önde gelen bir araç haline getirmiştir.

YH-AKM görüntüleme tekniğinin hızı ve tepkisi konsol probları, işletim ortamı, tarama teknikleri, vs., gibi çeşitli faktörler tarafından kısıtlanmıştır. Konsollar YH-AKM sistemlerinin vazgeçilmez ve dahili parçalarıdırlar, dolayısıyla, onların kendi kritik değerlendirilmeleri gerekir. Bu yüzden, rezonans frekansı, sertlik, ve Q-faktörü gibi çeşitli parametrelerin değerlendirilmesi aktif araştırma alanlarıdır.

Bu simülasyon tabanlı araştırma çalışması YH-AKM operasyonunun hava ve sıvı ortamlarında deneysel koşullarını taklit etmektedir. Ortamın viskoz ve akustik sönümlemesi, sıkma film sönümlemesi, ve malzemenin viskoelastisitesinden kaynaklanan sönümleme gibi sönümleme mekanizmaları sonlu eleman simülasyonlarına dahil edilmiştir. YH-AKM'ye uygun, sertlikleri ~1 N/m ve birinci normal titreşim modu rezonans frekansları ~1.5 MHz (sıvıda) ve ~5 MHz (havada) olan yüksek frekanslı yumuşak konsollar üzerine çalışılmıştır. Silisyum ve Polimer (SU-8) malzemeden yapılmış uzunlukları ~5 to 10 μm, genişlikleri ~1 to 2.5 μm, ve kalınlıkları ~0.1 to 0.6 μm aralıklarında olan çeşitli küçük dikdörtgen ve değiştirilmiş konsollar analiz edilmiştir. Bu araştırmada amacımız YH-AKM uygulamalarını uygun konsol geometrilerini ve malzemelerini tespit etmektir.

To My late Grandfather

Sardar Jaswant Singh Ghai

TABLE OF CONTENTS

LIST OF FIGURES

Figure **Page**

LIST OF TABLES

LIST OF SYMBOLS

µm ..... Micrometer

GPa ..... Giga Pascal Second

kg/m^3 ..... Kilogram per Meter Cube

MHz ..... Mega Hertz

N/m ..... Newton per meter

nm ..... Nanometer

ms ..... Millisecond

m/s ..... Meters per Second

Pa ..... Pascal

Pa.s ..... Pascal Second

b ..... Damping Factor

D_E ..... Diameter of Environment

D_{TS} ..... Distance between Substrate and Cantilever

E ..... Young's Modulus

E' ..... Storage Module

E'' ..... Loss Modulus

f_r ..... Resonance Frequency

f_{rl} ..... Resonance Frequency in Liquid

F ..... External Force

F_{tsi} ..... Tip Sample Interaction Force

k ..... Spring Constant

l ..... Length

m ..... Effective Mass

n ..... Mode Number

Q ..... Quality Factor

Q_{ankr} ..... Quality Factor due to Anchor Loss

Q_{aco} ..... Quality Factor due to Acoustic Damping

$Q_{coating}$ ..... Quality Factor due to Coating Loss

Q_{ext} ..... Extrinsic Quality Factor

Q_{int} ..... Intrinsic Quality Factor

Q_{VED} ..... Quality Factor due to Viscoelastic Damping

Q_{visc} .....Quality Factor due to Viscous Damping

Q_{sqz} .....Quality Factor due to Squeeze Film Damping

Q_{TED}.....Quality Factor due to Thermoelastic Damping

Q_{total}.....Total Quality Factor

t ..... Thickness

ω_r .....Angular Resonance Frequency

w..... Width

z.....Tip Displacement

|Z| .....Cantilever Oscillation Amplitude

θ .....Cantilever Angle

LIST OF ABBREVATIONS

AFM ..... Atomic Force Microscopy
ADP ..... Adenosine Diphosphate
AM ..... Amplitude Modulation
AM-AFM ..... Amplitude Modulation - Atomic Force Microscopy
ATP ..... Adenosine Triphosphate
BW ..... Bandwidth
DNA ..... Deoxyribonucleic Acid
FPS ..... Frames per Second
PD ..... Photodetector
HS-AFM ..... High-Speed Atomic Force Microscopy
M5 ..... Myosin 5
OBD ..... Optical Beam Deflection
Q-factor ..... Quality Factor
Si ..... Silicon
TED ..... Thermoelastic Damping

CHAPTER 1

INTRODUCTION

Since the invention of Atomic Force Microscope (AFM) by G. Binnig and his colleagues in 1986, it is now routinely used as a Nano tool for various measurements, for instance, it has been applied to biological samples such as proteins, nucleic acids, membrane lipids, live cells under physiological conditions. Recent development in AFM, i.e., High-Speed Atomic Force Microscopy (HS-AFM) technology especially in biological research has resulted in remarkable improvements. These advancements have offered possibilities to grasp the vibrant changes in the structure of the given biological samples directly and visualize the dynamic exchanges happening in them, which is not conceivable with any other methods.

HS-AFM is unique in its ability to observe surface topography of objects with the resolution of single atoms on solid surface. Various HS-AFM imaging studies have been done for direct observation of structure dynamics and dynamic processes of biological molecules in physiological solutions. In the past, range of efforts have been pointed at augmenting the resolution and speed. As the cantilevers play essential role in HS-AFM Imaging, the analysis of the resonance frequencies, spring constants, and Q-factors of the cantilever eigenmode is an active area of research.

The presented work concentrates on a complete and deep understanding of the effects of cantilever geometries and operating environments on resonance frequencies and Q-factors. This analysis allows us to propose improvements for multi-frequency and HS-AFM imaging techniques.

The second chapter, briefly examines the techniques and working principle of Atomic Force Microscopy. This chapter also presents HS-AFM studies and applications.

The third chapter presents the rectangular cantilever's mathematical point mass model and its basic properties, i.e., quality factor (Q-factor), resonance frequency (f_r) and the spring constant (k).

Chapter four provides general idea about the simulation model. In addition, it discusses damping mechanisms.

Chapter five elaborates the results calculated for Silicon and SU-8 cantilevers and the effect of environment on cantilever resonance frequencies and quality factors.

Furthermore, this section explores the effects of modified geometries on the resonance frequencies and Q-factors.

The last chapter gives conclusions on the performed simulations and an understanding their implications on HS-AFM imaging.

CHAPTER 2

HIGH-SPEED ATOMIC FORCE MICROSCOPY

In 1981, Invention of Scanning Tunnelling Microscope opened up new category of instruments to measure surface topographies at atomic level (Binnig and Rohrer 1983). Three years later, another technique named Atomic Force Microscopy (AFM) is introduced (Binnig, Quate, and Gerber 1986). Atomic Force Microscopy's unique ability to observe surface topography of the samples with height data and capturing high resolution images makes it a prominent tool in Nano measurements. This microscopy technique has gone through many technical and scientific developments, plenty of instrument variations have been introduced and used in wide range of applications from physics of surface to material science, microelectronics, biology and chemistry.

Before the invention of AFM, the visualization of biological samples (proteins, membrane lipids, DNA) was only possible in vacuum environment by electron microscopy. Since then various AFM imaging studies have been done to explore the potential to obtain high resolution images. Atomic Force Microscopy was expected to bridge a gap between single-molecule biophysics and structural biology. However, even AFM's unique capability of high-resolution visualization failed to answer some significant questions related to dynamics of biological samples in liquid environment. As the functions of biological samples are dynamic in nature, AFM is required to capture those dynamic processes rapidly with series of very fast high-resolution images. Nevertheless, the rate of imaging in traditional AFM is remarkably slow to seize the dynamic behaviour of biological samples.

2.1. Operating Principle of AFM

A basic schematic representation of AFM is depicted in the Figure 2.1. AFM acquire the series of images by probing the surface of sample with a sharp cantilever tip. To identify the cantilever beam's deflection, an optical beam deflection (OBD) detection method is used. At the free end of the cantilever a laser beam is focused and reflected back to a photodetector (PD). The scanning of the sample stage is done with a classic raster mode scanning, during this operation, the detected deflection of the cantilever is

compared to the set point. This whole operation is shown in Figure 2.1, is a closed-loop feedback system which helps maintain the cantilever's deflection at the reference point. As a result, the sample stage moves in three dimension which leads to depict the sample's surface with the height data. Thus, a topographical image of the sample's surface can be obtained.

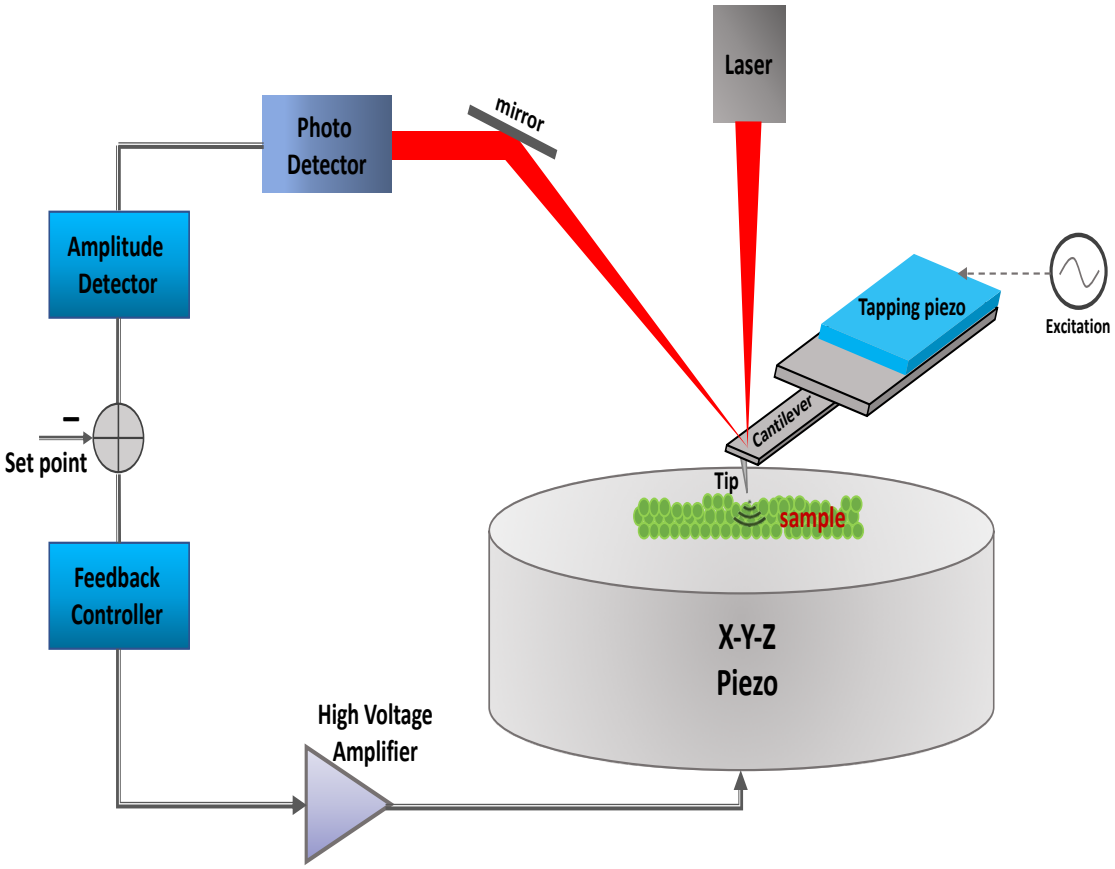

Figure 2.1. Schematic of atomic force microscopy setup.

2.1.1. Modes of Operation

To understand the basic difference of the operating modes, first a brief introduction to tip surface interaction forces (F_{tsi}) is given. Figure 2.2 depicted a graph of F_{tsi} as a function of the tip-sample distance (D_{ts}) between the cantilever tip and sample. A positive interaction force in the graph stands for, when a repulsive force pushes the cantilever tip away from the sample, as a result, there is a positive deflection of cantilever in z-direction. A negative interaction stands for an attractive force pulling the cantilever tip towards the surface of sample, as a result, there is a negative deflection of the cantilever.

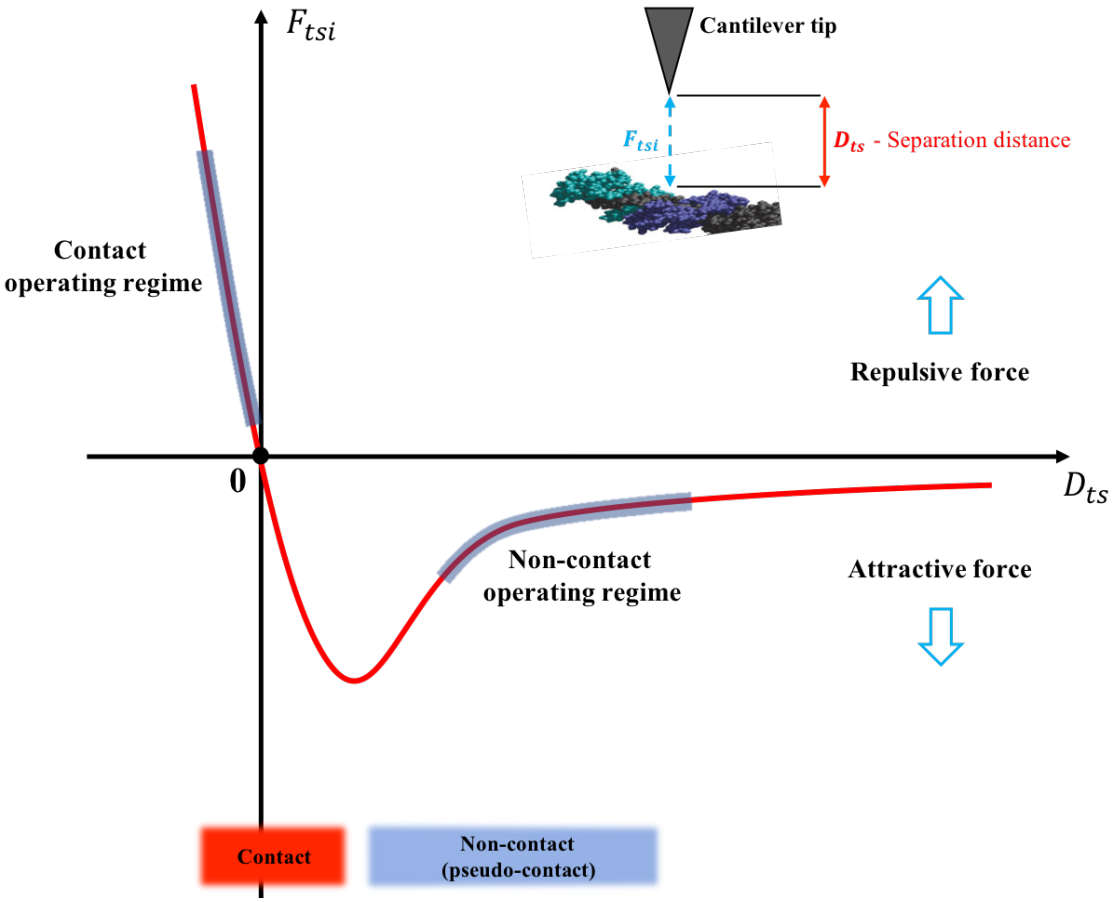

Figure 2.2. Interaction force and operating regime in HS-AFM as a function of tip sample distance.

2.1.1.1. Contact Mode

Contact mode (Fig. 2.3) was the first mode developed for the AFM. The cantilever in this mode is directly in contact with the surface of the sample to be scanned. The repulsive interaction force is determined by static deflection of the cantilever. Between tip and surface a strong repulsive interaction force and friction are present.

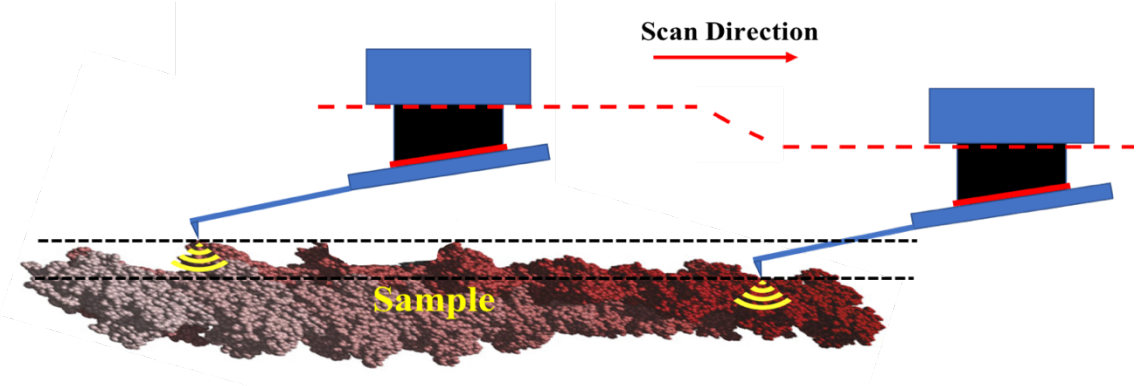

Figure 2.3. Contact mode.

Due to repulsive force the sample may be damaged by this scanning process. As sample surface and the cantilever's tip are constantly in contact during the scanning process, lateral force is also sensed by both sample and the cantilever's tip.

2.1.1.2. Tapping Mode

In 1987, Martin *et al.* invented the tapping mode for atomic force microscopy (Martin, Williams, and Wickramasinghe 1987). The cantilever tip no longer maintains the contact with sample surface, i.e., the tip strikes or taps the sample periodically. Since the tip is no longer dragged along the surface, tapping mode decreases the shear force exerted on the sample surface.

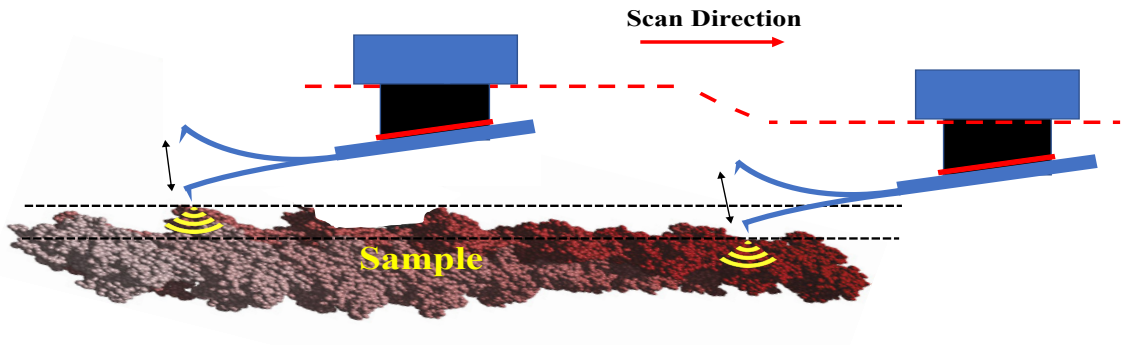

Figure 2.4. Tapping mode.

In this mode, the cantilever is oscillated at or near its natural frequency in *z*-direction. The cantilever driver used in this mode is usually a piezo-electric element. When the oscillated cantilever tip taken closely to the sample surface, the oscillation amplitude changes due to F_{tsi}. The reduction in amplitude is closely monitored and the sample piezo adjusts the height in *z*-direction via the feedback loop. Since, this mode monitors the changes in oscillation amplitude, it is also known as Amplitude Modulation AFM (AM-AFM).

2.2. HS-AFM Studies and Applications

Since the availability of HS-AFM, the number of studies related to HS-AFM imaging in the field of Nano and biosciences have rapidly increased. HS-AFM addressed the issues which had been difficult or impossible to tackle in biological research.

Studies till now have covered extensive range of structure dynamics and active molecular processes. These studies have been categorized in accordance with protein or biological systems' conformational changes (Shibata *et al.* 2011) (Noi *et al.* 2013) (Uchihashi *et al.* 2011); motor actions (Kodera *et al.* 2010); DNA-protein interactions (Miyagi, Ando, and Lyubchenko 2011), diffusions and interactions in membranes and on live cell surfaces (Colom *et al.* 2012) (Yamashita *et al.* 2009) (Yamashita *et al.* 2012); self-assembly processes (Yilmaz *et al.* 2013); enzymatic reactions (Igarashi *et al.* 2011); and dynamics occurring in intrinsically disordered proteins (Suzuki *et al.* 2011) (Hashimoto *et al.* 2013).

In above mentioned areas, most astonishing results have been obtained in the observation of conformational changes of myosin V (M5-HMM) molecule (Kodera *et al.* 2010). The hand-over-hand movement of the myosin V molecule, which was previously only speculated, has been observed through HS-AFM with a visual evidence. The myosin V motor molecule's study reveals detailed behaviors like unidirectional processive movement, lever-arm swing leads to an extensive insight of motor structure.

In the experiment, house-built tapping mode high-speed atomic force microcopy with high frequency small cantilever was used. A cantilever, with a resonance frequency of 1.2 MHz (in liquid), spring constant of 0.2 N/m, was used to facilitate the high-speed operation. In addition, a tip on the small cantilever was grown by electron-deposition method and was further sharpened to achieve the radius of ~4 nm by argon plasma etching technique. The experiment was performed at room temperature, for ease of operation, the sample area was chosen such a way that the actin filaments were parallelly aligned in *x*-direction. The high precision feedback system of HS-AFM and the property of Myosin V (strolls straight along with actin filaments) facilitates the continuous imaging of the walking Myosin V molecule. Imaging rate of 146.7 ms per frame was achieved which is sufficient to capture the dynamic Myosin V molecule.

Another HS-AFM study discloses Rotary Catalysis of Rotorless F_1-ATPase (Uchihashi *et al.* 2011). F_1-ATPase, a water dissolvable fragment of adenosine triphosphate (ATP) synthase (*I*), is a spinning motor protein. ATP synthase is an essential catalyst which generates the energy storage molecule adenosine triphosphate (ATP). For various organisms, ATP is a popular energy currency. ATP is formed with the help of adenosine diphosphate (ADP) and inorganic phosphate (Pi), and it needs energy for its composition. The $\alpha_3\beta_3\gamma$ sub-complex (referred as a F_1) suffices as

motor, where the rotor γ spins in the stator $\alpha_3\beta_3$ ring at the time of ATP hydrolysis. The catalytic sites in F_1 are primarily detected at β subunits. The three catalytic sites are in distinctive nucleotide bound states; one connects to an ATP analog, i.e., α_{TP}-$\beta_{TP;}$ second connects it to adenosine diphosphate (ADP), i.e., α_{DP}-β_{DP}; the 3rd remains unbounded, i.e., α_E-β_E. Traditional optical microscopy does not permit to visualize whether the intrinsic cooperativity in the $\alpha_3\beta_3$ ring is the core element accountable for subsequent torque generation. The authors clarify the same affair with the help of HS-AFM by directly envisioning the ATP-driven conformational shift of β's in the confined $\alpha_3\beta_3$ ring. The $\alpha_3\beta_3$ sub-complex was covalently incapacitated on a surface of mica and examined with high-speed atomic force microscopy with an imaging rate of 80 ms per frame.

Furthermore, HS-AFM is being used for industrial scale materials characterization (Payton, Picco, and Scott 2016) (Seong *et al.* 2014) (Braunsmann and Schäffer 2010) (Payton *et al.* 2016) (Cullen *et al.* 2016). Recently, to study corrosion, HS-AFM was used to depict the microstructure of AGR fuel cladding and Magnox (Laferrere *et al.* 2017). A. Pyne *et al.* studied artificial and actual dental enamel in both neutral and acidic aqueous environments using HS-AFM with small cantilevers of high resonance frequency ~1 MHz (Pyne *et al.* 2009). Another study by T. Itani *et al.* was conducted on characterization of photoresist solution using HS-AFM imaging technique, a small cantilever with resonance frequency of 1 MHz in liquid and a spring constant of 0.1-0.3 N/m was used in this experiment (Itani and Santillan 2010).

CHAPTER 3

CANTILEVERS AND THEIR PROPERTIES

The cantilevers are indispensable and integral part of HS-AFM. The modern day micro sized cantilevers were first invented and used for the AFM application by Wolter *et al.* (Wolter, Bayer, and Greschner 1991) and Quate *et al.* (Akamine, Barrett, and Quate 1990) (Tortonese, Barrett, and Quate 1993). With the advancement in the fabrication techniques, there exist various types of cantilever beams with variety of shapes. In most of the AFM studies, rectangular cantilever beams (Fig. 3.1) are being used.

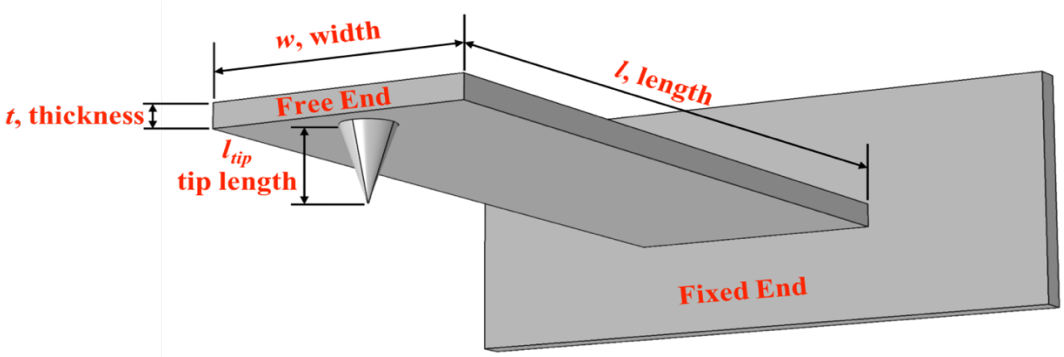

Figure 3.1. Schematic of a rectangular beam with tip at the free end.

A large commercial rectangular cantilever (approx. l = 200 µm, w = 50, t = 10 µm) is used for the conventional atomic force microscopy imaging. However, for high-speed AFM operations, a small rectangular cantilever (approx. l = 7 µm, w = 2.5 µm, t = 0.2 µm) is used. A side by side comparison of large and small commercial AFM cantilevers is shown in Figure 3.2.

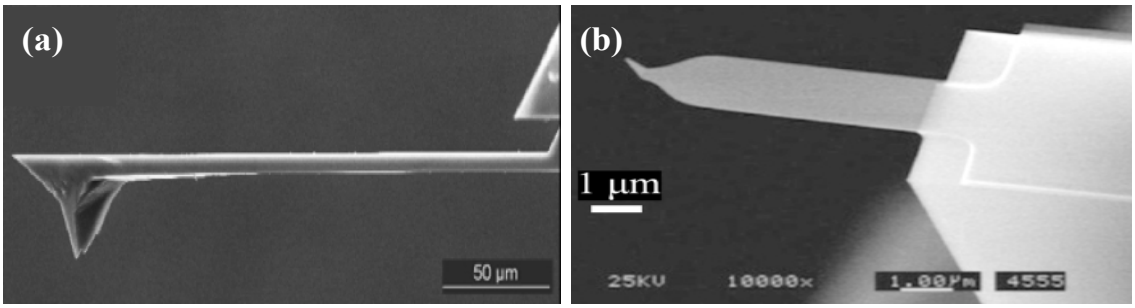

Figure 3.2. Comparison between commercially available large and small AFM cantilevers. (Source: Calabri *et al.* 2008, Ando 2012).

3.1. Flexural Eigenmodes

The cantilever beam used in tapping-mode imaging has to be excited at a certain frequency and the vibration caused by this excitation has to be identified. There are variety of excitation methods available, and they all have their corresponding detection methods.

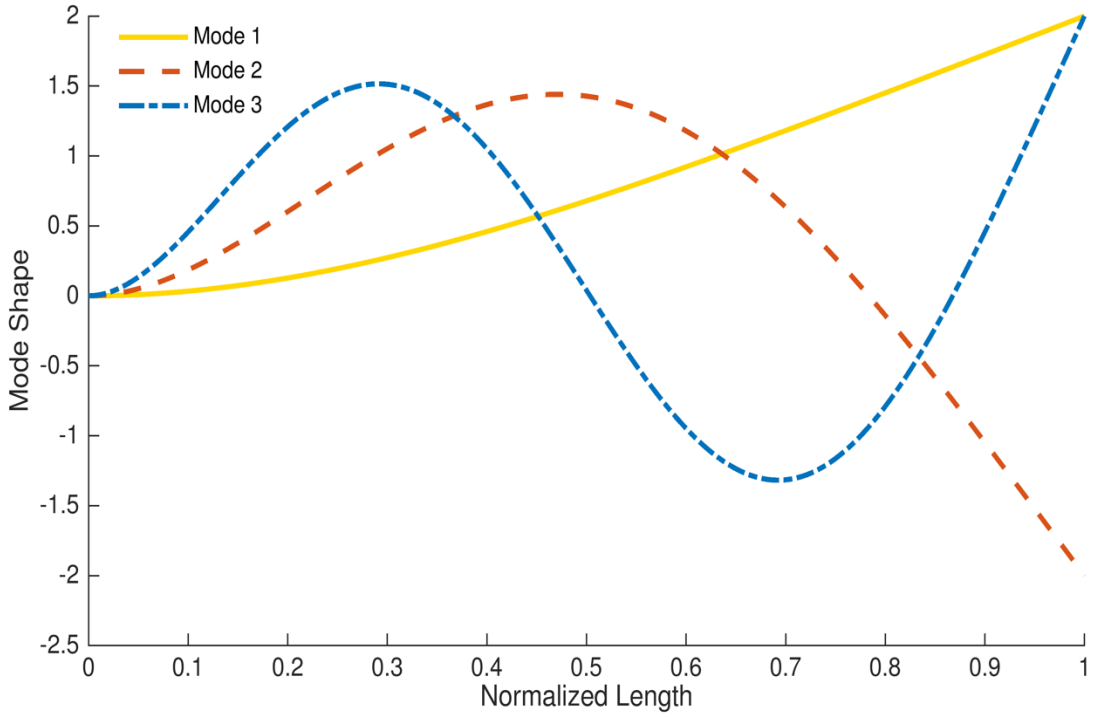

Figure 3.3. Flexural Eigenmode shapes calculated in MATLAB.

Every cantilever, regardless of its shape, has its own displacement pattern, *Q*-factor and resonance frequency. The cantilever has three different vibration modes, i.e., flexural, torsional and lateral mode. Each cantilever has multiple higher-order resonance frequencies. For a rectangular cantilever first three flexural modes are calculated in MATLAB and are shown in Figure 3.3.

3.2. Point-Mass Model

The dynamic behavior of a cantilever can be explained simply by a mathematical point mass model. For the dynamic operation mode, it is considered as an adequate model.

The mechanical performance of the cantilever can be expressed by 2nd order differential equation.

$$m\ddot{z} + b\dot{z} + kz = F \tag{3.1}$$

where, m is the effective cantilever mass, b is the damping factor, k is the spring constant, z is the deflection of mass and F is the external force acting on the cantilever.

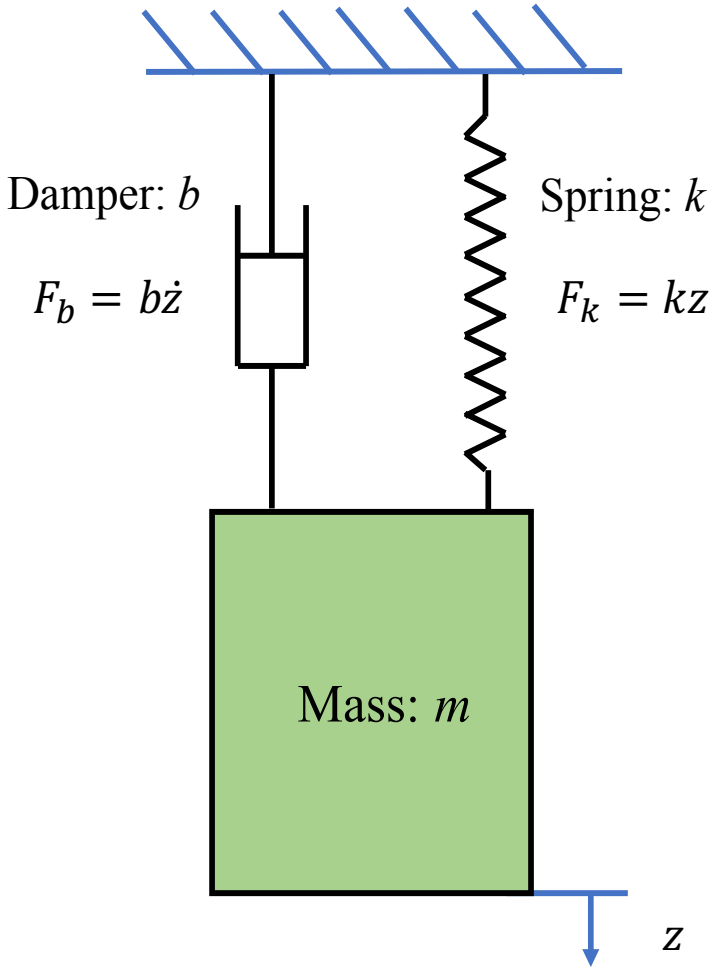

Figure 3.4. Free vibration of a cantilever represented as a mechanical point mass model with spring (k), damper (b) and mass (m).

3.3. Resonance Frequency (f_r) and Quality Factor (Q)

For high-speed atomic force microscopy operation, a high imaging bandwidth is required. Therefore, a small cantilever with a frequency larger than 1 MHz is desired. The resonance frequency is given by

$$f_r = \frac{1}{2\pi}\sqrt{\frac{k}{m}} \tag{3.2}$$

where m is the effective mass and k is the spring constant of the cantilever.

The damping coefficient (b) is given by

$$b = \frac{m\omega_r}{Q} \tag{3.3}$$

By inserting Equation 3.3 into Equation 3.1 and re-arranging the terms the cantilever oscillation amplitude $|Z|$ as a function of frequency is obtained.

$$|Z| = \frac{|F|/k}{\left[\left(1 - \frac{\omega^2}{{\omega_r}^2}\right)^2 + \left(\frac{\omega}{\omega_r Q}\right)^2\right]^{1/2}} \tag{3.4}$$

There are certain variables like the environment where the cantilevers are constantly immersed, and the dimensions that strongly affect the resonant frequencies and Q-factors. The detection bandwidth $(B.W.)$ has a significant impact on the imaging speed of high-speed atomic force microscopy. The bandwidth is closely related to the cantilever's resonance frequency (f_r) and Q-factor $(B.W. \propto f_r/Q)$, it is a measure of maximum rate of change in topography a cantilever can precisely detect.

Figure 3.5 depicts the amplitudes of cantilever oscillation for the same k and f_r at low, medium, and high Q-factors. Figure 3.6 shows the experimental result up to 20 MHz, carried out by Nievergelt *et al.* (Nievergelt *et al.* 2014). It shows the first three flexural and first two torsional modes of a rectangular beam.

For a damped cantilever, the Q-factor in terms of energy (Blom *et al.* 1992), is given as

$$Q = \frac{2\pi\ (stored\ vibration\ energy)}{dissipated\ energy\ per\ period} \tag{3.5}$$

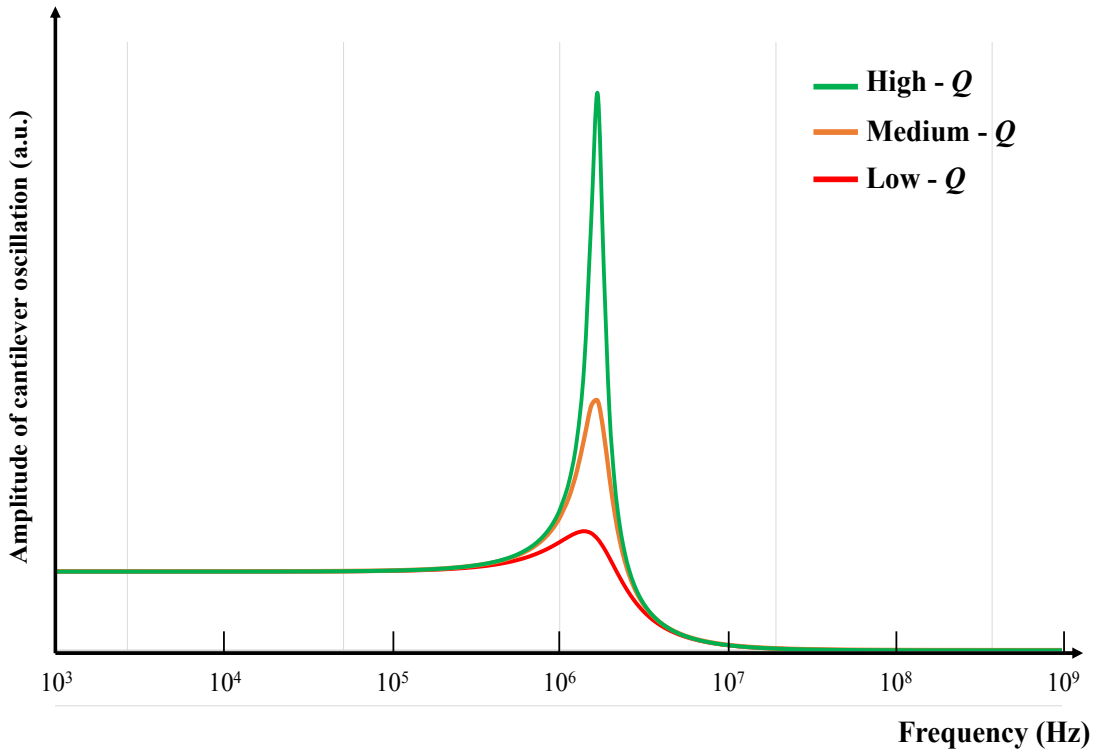

Figure 3.5. Comparison of *Q*-factors for the same spring constant and resonance frequency.

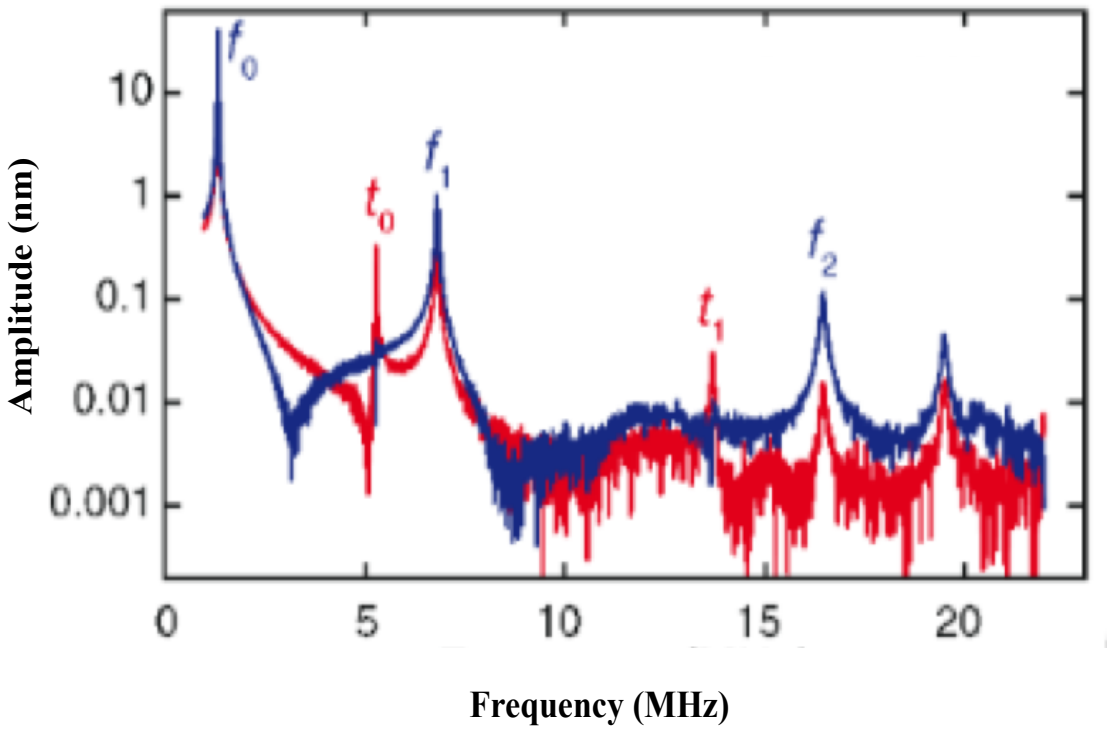

Figure 3.6. Experimental results of amplitude response with respect to frequency of a rectangular cantilever showing first three flexural modes. (Source: Nievergelt *et al.* 2014).

For HS-AFM, typical value of Q-factor in water varies from 2 to 5 and in the air, it varies from 40 to 300. In HS-AFM, quality factor determines the settling time of the cantilever, which can be deemed as limiting parameter to the measurement bandwidth.

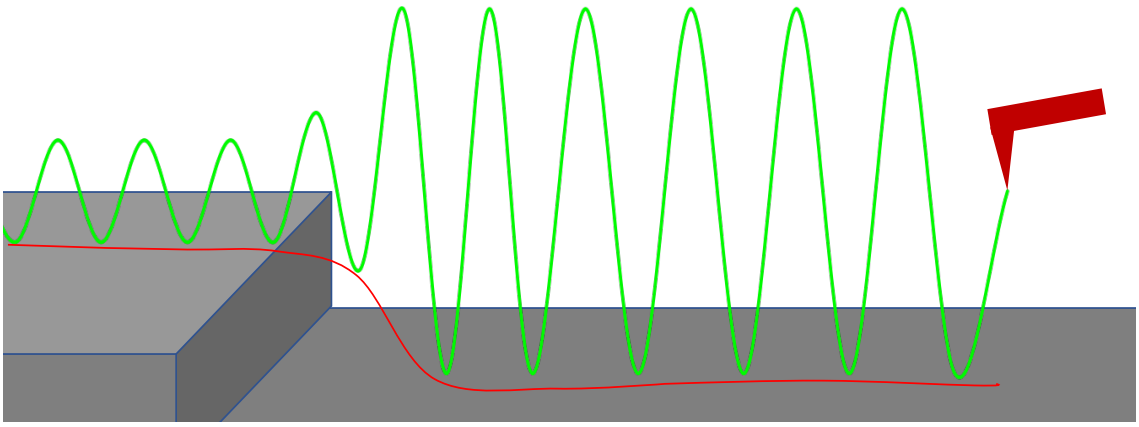

Figure 3.7. Low resonance frequency with low Q-factor.

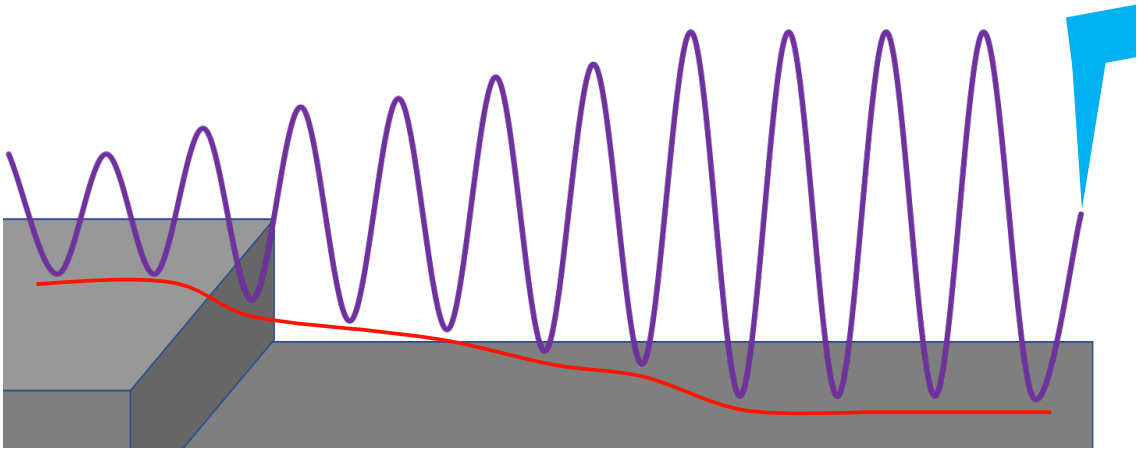

Figure 3.8. Low Resonance frequency with high Q-factor.

For high force sensitivity, a high Q-factor is required, however, low Q-factor is needed to obtain high bandwidth. Sensitivity at the expense of bandwidth is a trade-off, which ultimately depends on the application. A cantilever with a low and a high Q-factors with a low resonance frequency (f_r) are shown in Figure 3.7 and 3.8, respectively. When the cantilever oscillates at its resonance frequency and when it experiences a change in topography while scanning the sample, it requires certain amount of cycles to reach its new steady-state amplitude.

In an ideal HS-AFM imaging, from the perspective of faster imaging and high detection bandwidth, i.e., fastest amplitude response, a cantilever is required with high

resonance frequency (f_r) and low Q-factor. A cantilever with a low and a high Q-factors with a high resonance frequency (f_r) are shown in Figure 3.9 and 3.10, respectively.

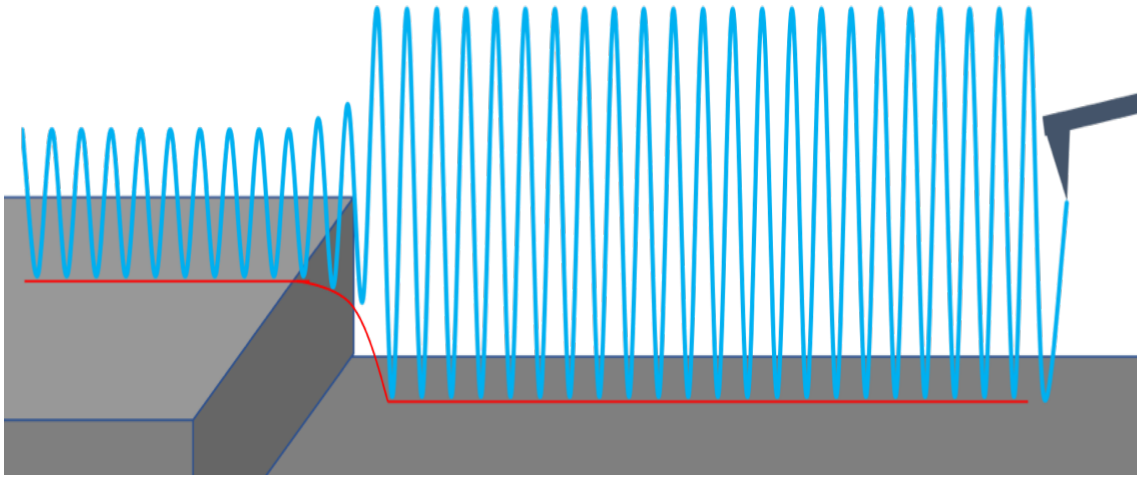

Figure 3.9. High resonance frequency with low Q-factor.

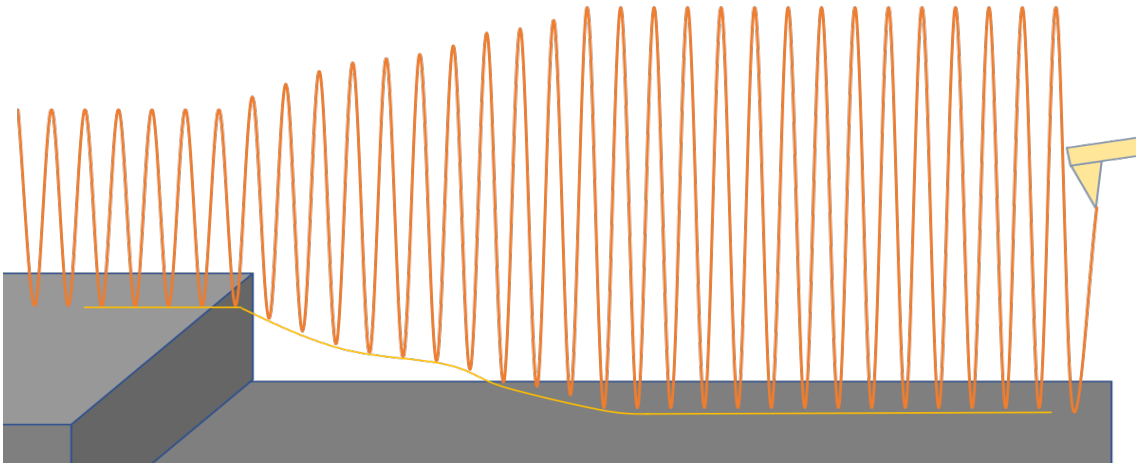

Figure 3.10. High resonance frequency with high Q-factor.

3.4. Spring Constant (k)

Certain properties of a small rectangular beam are the key parameters responsible for its performance. One of the parameters is spring constant (k). It can be measured using material properties and dimensions of cantilever. The spring constant (k) of a rectangular cantilever is given by

$$k = \frac{Ewt^3}{4l^3} \tag{3.6}$$

where, E, l, w and t are Young's modulus, length, width and thickness of a rectangular cantilever respectively.

For biological samples, low spring constant (k) cantilevers are desired in order not to damage the samples. To achieve both low spring constant (k) and high resonance frequency (f_r) the cantilever has to be small.

CHAPTER 4

SIMULATION MODEL

With the continuous immersion of the cantilever in liquid or air environment, this study needs a simulation model, which can accurately illustrate the high-speed atomic force microscopy operation and calculates various parameters of cantilever by taking into account various factors like viscosity, pressure, density, damping etc.

4.1. Typical HS-AFM Setup

The cantilevers for the HS-AFM operation, continuously immersed in the liquid or air environment shown in Figure 4.1 and the surrounding environment has subtle influence on cantilever beams.

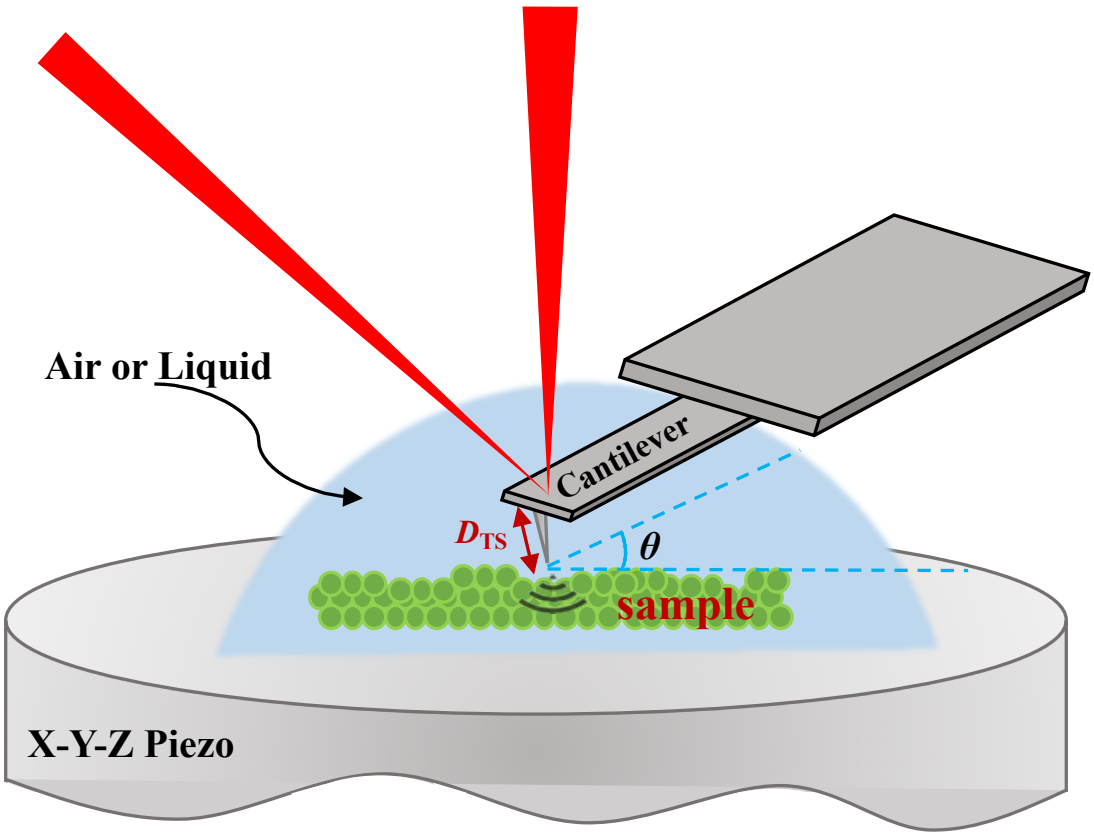

Figure 4.1. Close-up view of tip-sample interaction in a typical HS-AFM experiment.

Most of the cantilever characteristics, i.e., resonance frequency (f_r), Q-factor and spring constant (k) can be directly determined from the mechanical dimensions of the beam and from known material properties. The basic properties for Silicon (Si) and SU-8 polymer are shown in the Table 4.1.

Table 4.1. Basic material properties.

Material	Properties		
	Young's Modulus GPa	Density kg/m³	Poisson Ratio
Silicon	170	2330	0.28
Polymer (SU-8)	4	1200	0.22

4.2. Model Geometry

A model of the high-speed atomic force microscopy system is shown in Figure 4.2. The cantilever beam and the substrate are made by silicon or SU-8 material and are surrounded by fluid (air or liquid).

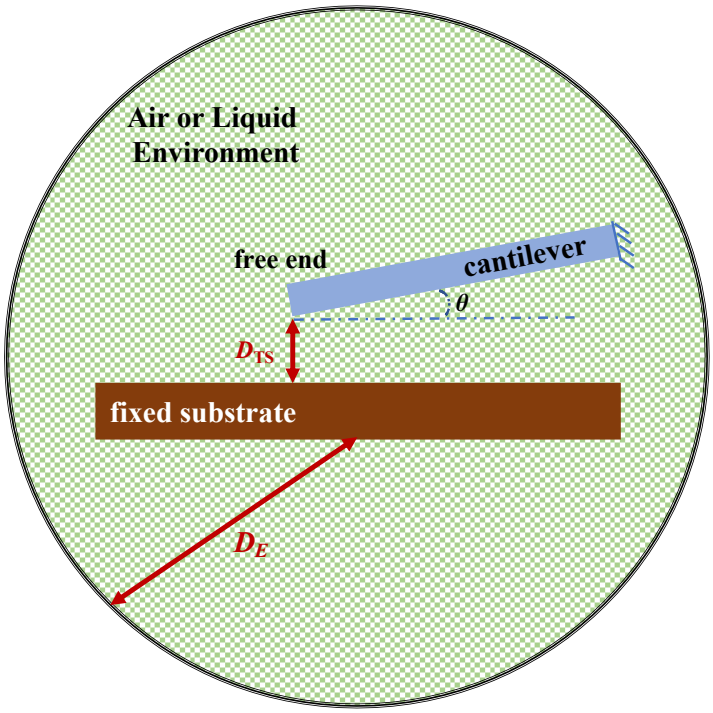

Figure 4.2. Model geometry.

The cantilever is fixed at one end, whereas, the substrate at a distance (D_{TS}) of 2 µm from the cantilever's free end, is fixed on all sides. D_E is taken as 50 µm. To make the simulation model more realistic, an angle (θ) of 10° is kept between the cantilever and substrate. The substrate modeled in this geometry, is assumed as a sample holder. The model is designed to get the correct assessment of the factors affecting the deflection of cantilever beam, i.e., damping, viscosity, pressure.

4.3. Damping Factors

In general, when the cantilever beam operates in a vacuum environment, only intrinsic losses ${Q_{int}}^{-1}$ are in effect. Intrinsic losses contain viscoelastic damping ${Q_{VED}}^{-1}$ in the cantilever beam, damping due to fixing the cantilever end, i.e., anchor loss ${Q_{ankr}}^{-1}$, coating loss ${Q_{coating}}^{-1}$ due to film coating of cantilever and thermoelastic damping ${Q_{TED}}^{-1}$due to thermoelastic properties of material. When the cantilever beam operates in air or liquid environment, external losses ${Q_{ext}}^{-1}$ affects the Q-factor. The external losses consist of squeeze film effect ${Q_{sqz}}^{-1}$, acoustic losses ${Q_{aco}}^{-1}$, and viscous losses ${Q_{vis}}^{-1}$. Therefore, the total ${Q_{total}}^{-1}$ is the sum of all these losses.

$$ {Q_{total}}^{-1} = \underbrace{{Q_{VED}}^{-1} + {Q_{ankr}}^{-1} + {Q_{coating}}^{-1} + {Q_{TED}}^{-1}}_{{Q_{int}}^{-1}} + \underbrace{{Q_{sqz}}^{-1} + {Q_{aco}}^{-1} + {Q_{visc}}^{-1}}_{{Q_{ext}}^{-1}} \tag{4.1} $$

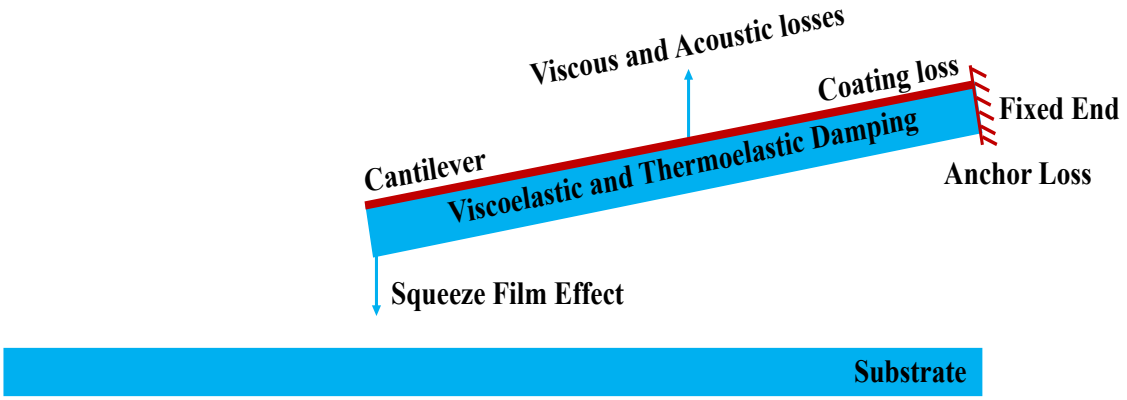

Figure 4.3. Various losses of cantilever.

Figure 4.3 shows various damping factors that may affect the cantilever's *Q*-factor. For this study, viscous losses of the medium, acoustic losses, squeeze film damping due to nearby substrate, and viscoelasticity losses due to cantilever material are taken into account. Coating loss, anchor loss and thermoelastic damping (TED) are ignored.

4.3.1. Squeeze Film Damping

The damping effect of the surrounding environment (air or liquid) would be increased when the cantilever oscillates near a second surface (fixed substrate in this case) due to pumping action of environment between the surfaces (Newell 1968) (Andrews, Harris, and Turner 1993) (Bao and Yang 2007). In numerous HS-AFM applications, cantilevers are oscillating near a fixed substrate, therefore, the squeeze film damping factor immensely influences the *Q*-factors.

4.3.2. Viscous Damping

In the viscous region the air or liquid acts as a viscous fluid and the drag force must be calculated using fluid mechanics. When the gas flow is considered as incompressible, since the velocity of oscillating beam is smaller than the speed of sound in the medium and the viscous drag is typically dominant liquid damping mechanism (Blom 1992). The effect of viscous damping on cantilever's *Q*-factor is taken into account for this study.

4.3.3. Acoustic Damping

At high frequencies, the acoustic losses may dominate the *Q*-factor of a cantilever. For this study small high frequency cantilevers are used, as the eigenmode frequency increases, the acoustic wavelength becomes closer to spatial wavelength of the cantilever beam and the compressibility comes into consideration (Qiu 2014). Therefore, the energy dissipation by acoustic waves is also included while calculating the *Q*-factors.

4.3.4. Anchor Loss

Anchor loss regards to the mechanical energy that is dissipated via the coupling to the fixed end (or support structure) of the cantilever. When the cantilever oscillates, it exerts the fixed end with the small deformations, thereby leading to generation and propagation of elastic waves to the material. Therefore, the fixed end absorbs some of the oscillation energy of the cantilever. It certainly has an impact on the *Q*-factor of the cantilever, however, for this study anchor losses are neglected.

4.3.5. Thermoelastic Damping

The thermoelastic damping (TED) is another energy loss factor, which impacts the *Q*-factor of a cantilever beam. When the cantilever vibrates at its resonance frequency, a strain gradient is produced, which causes temperature gradient and yields the heat flow. Therefore, the energy is dissipated due to deformation of the cantilever. If the oscillation frequency is of the order of the heat relaxation rate, the energy loss becomes noticeable due to thermoelastic damping, which decreases the *Q*-factor. Thermoelastic damping limits the *Q*-factor in vacuum environment. Since we model the HS-AFM setup in air and liquid environment its effect is negligible and it is not taken into account.

4.3.6. Damping by Thin Film Coating

For numerous applications, the cantilevers are coated with thin films to sense electrical functions (Qiu 2014), or to modify the surface chemistry (Fadel *et al.* 2004), or to supply optical reflectivity (Meyer and Amer 1988). Due to thickness of coating and internal friction between/in each coating layer, a decline in *Q*-factors has been observed (Sandberg *et al.* 2005) (Sekaric *et al.* 2002). However, for this study, due to absence of any kind of coating, the damping by thin film coating is ignored.

4.3.7. Viscoelastic Damping

In any material, the energy is dissipated due to internal friction of the molecular friction, which ultimately affects the *Q*-factor of the cantilever. Viscoelastic damping is

mainly caused by the material properties and is accounted in this study to calculate *Q*-factors for rectangular cantilever. The viscoelastic effect, due to complex nature of Young's modulus on *Q*-factors is also taken into account for the SU-8 material (Adams et al. 2015).

CHAPTER 5

RESULTS AND DISCUSSION

The demonstrated simulation model in the study mimics the actual working model of high-speed atomic force microscopy. The cantilevers possess multiple eigenmodes of vibration with their own natural frequency. A detailed evaluation of the frequency response of series of small, high frequency cantilevers are discussed in this section. The work simultaneously measures and compares various effects of surrounding fluid, geometry modification, materials and presence of a nearby surface (squeeze film effect).

5.1. Comparison to Prior Studies

A needful comparison with certain prior studies has been made in order to ensure the validity of the simulation model outcome. Numerous simulations with different rectangular cantilevers and environments are performed and the respective results are compared with the prior studies.

5.1.1. Silicon Cantilever

A micro-sized silicon rectangular beam with the geometrical dimensions of the length 2200 μm, width 400 μm and thickness of 22 μm is simulated. Figure 5.1 demonstrates the eigenfrequencies of the first three flexural eigenmodes of a rectangular cantilever beam.

The eigenfrequency results obtained by the proposed simulated model are well matched with the simulation and experimental results of the literature (Qiu 2014). A small percentage error of 4-5 in all the three eigenmode eigenfrequencies between simulation and literature is recorded. While comparing the experimental and simulation results, as the number of eigenmodes increases the percentage error is down to 0.8.

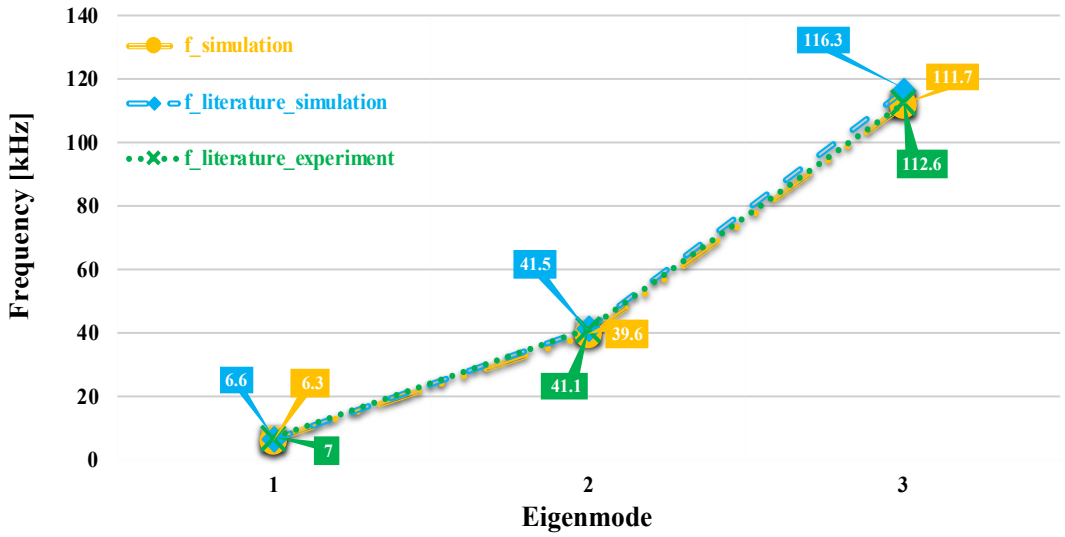

Figure 5.1. Comparison of flexural eigenmode frequencies obtained from simulation and the literature (simulation and experiment) (Qiu 2014).

5.1.2. *Q*-factor Dependence on Gap Width (Squeeze Film Effect)

To mimic the practical HS-AFM, a fixed substrate is placed at a distance of 2 µm from the free end of the cantilever. The substrate imitates the sample. To understand how fluidic dissipation is modified and how it affects the resonance frequency (f_r) and *Q*-factor, numerous simulations are performed at different gap widths (D_{TS}). The simulation is performed with the same cantilever beam as discussed in previous section.

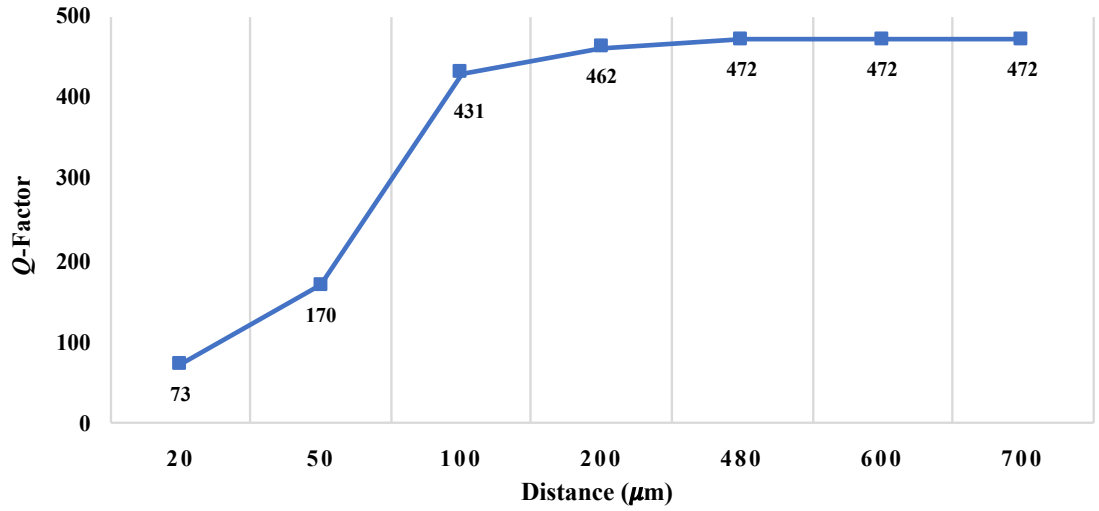

Figure 5.2. *Q*-factor variation with respect to substrate distance from cantilever beam.

The measured results match well with the literature (Qiu 2014). The resonance frequency (f_r) is almost insensitive to presence of substrate. However, as the distance (D_{TS}) between cantilever and substrate is decreasing, the squeeze film damping continues to affect the Q-factor. As shown in the Figure 5.2, Q-factor starts to increase with the increase in the gap width and after 480 µm distance, squeeze film effect has a very small influence.

5.1.3. Q-factor Dependence on Pressure

Depending on the pressure level, two different regimes are identified, i.e., molecular regime and viscous regime. The molecular regime varies from 1 Pa to 100 Pa (Blom 1992), where the damping is caused by collisions of air molecules with the moving surface of the vibrating cantilever. Whereas, viscous regime varies from 100 Pa to 100 kPa, the gas in this state acts as a continuous viscous fluid and the viscous drag dominates the loss mechanism. As the pressure varies to high vacuum region, gas damping become less effective hence the Q-factor is determined by the intrinsic damping of the cantilever.

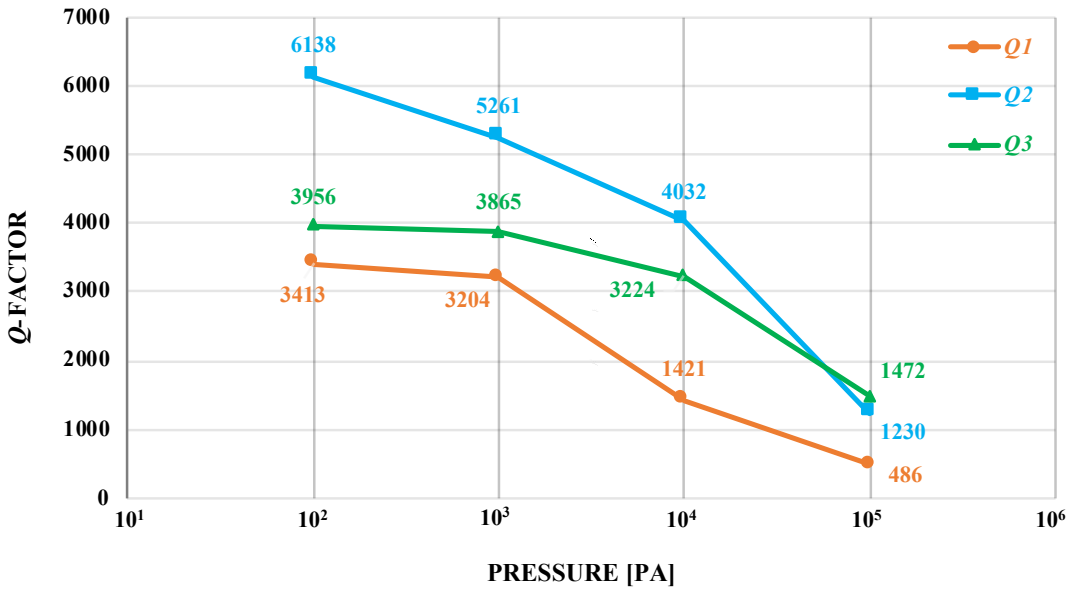

Figure 5.3. Q-factors variations of first three eigenmodes with respect to pressure.

For this study, as shown in Figure 5.3, Q-factors of first three flexural modes of a rectangular beam at different pressure levels are observed in unbounded state, i.e., absence of substrate. The calculated simulation results match well with the experimental

data provided in the literature (Qiu 2014). The results clearly indicate the Q-factors are very sensitive to density and the viscosity (Mertens *et al.* 2003) (Suzuki, Enoki, and Akiba 2004) of the surrounding fluid.

5.1.4. Small Cantilever in Air and Liquid

As simulation model determines correct resonance frequencies of the large rectangular cantilever beam, the next step is to analyze the small cantilever for high-speed atomic force microscopy. For this purpose, a commercial small high frequency cantilever (BL-AC7DS-KU2) custom-made by Olympus and used in home-made HS-AFM equipment to study and record real-time structure dynamics and dynamic processes of protein (Uchihashi, Kodera, and Ando 2012) is analyzed. The dimensions of the analyzed cantilever are 6 µm in length, 2 µm in width and 90 nm in thickness. Key parameters like first resonance frequency (f_r), Q-factor and the spring constant (k) are calculated.

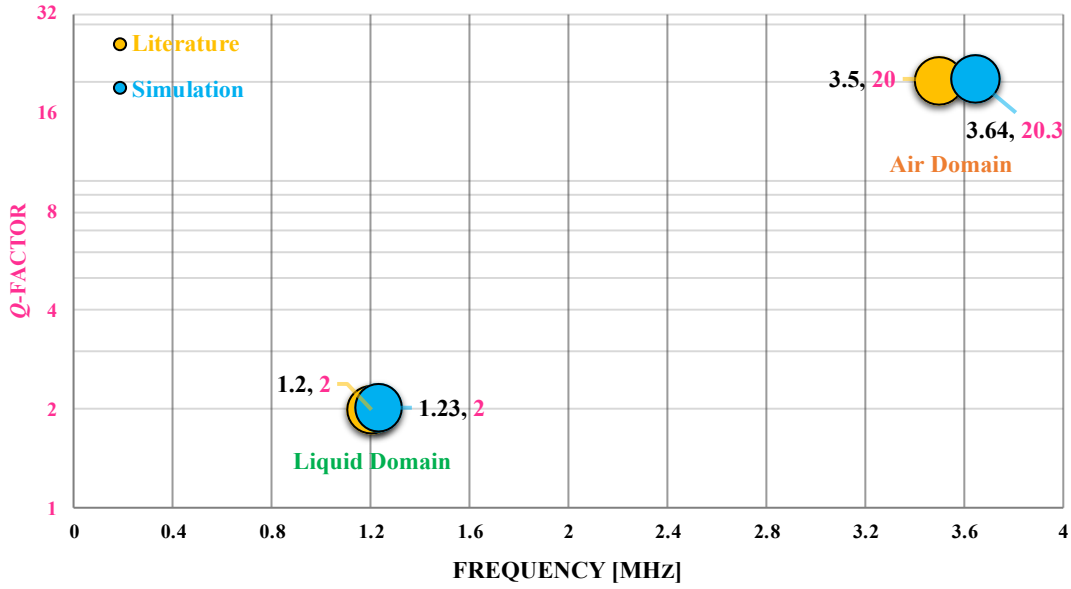

Figure 5.4. First eigenmode resonance frequency and Q-factor calculations of the commercial rectangular cantilever and the literature data (Uchihashi, Kodera, and Ando 2012).

Figure 5.4 shows a comparison of first eigenmode resonance frequency and Q-factor results in air and liquid environment for a commercially available cantilever with simulated results. A trivial percentage error in resonance frequency and Q-factor is recorded between simulated and available literature. In addition, the spring constant (k)

of 0.2 N/m is also calculated which the matches well with the literature (Uchihashi, Kodera, and Ando 2012).

5.2. High Frequency Silicon Cantilevers

By keeping the high-speed atomic force microscopy operation in mind, the study focuses on high resonance frequency (f_r) cantilevers. Therefore, a fixed first resonance frequency (f_r) of 1.5 MHz (± 10 %) in liquid environment, a 5 MHz (± 10 %) fixed first resonance frequency (f_r) in air environment and, a spring constant (k) of 0.9 N/m (± 10 %) is maintained while selecting the cantilever dimensions.

5.2.1. Air Environment

HS-AFM's wide variety of applications certainly makes the selection of cantilevers a difficult job. This section explores the effect of cantilever geometry on the Q-factors and resonance frequencies for the first three flexural eigenmode of the cantilever.

5.2.1.1. Rectangular Cantilevers

For a fixed first resonance frequency certain rectangular geometrical dimensions are simulated. The cantilever dimensions are given in Table 5.1. The spring constant (k) of 0.9 N/m (± 10%) for these rectangular cantilever dimensions is recorded.

Table 5.1. Rectangular cantilever dimensions.

Type	Length (µm)	Width (µm)	Thickness (µm)
Si Cantilever 1	5.5	2.6	0.11
Si Cantilever 2	6	2	0.13
Si Cantilever 3	6.7	1.5	0.16

The Figure 5.5 demonstrates the first three eigenmode frequency results of three different sized (Thinner, Moderate, Thicker) rectangular cantilevers. The eigenfrequency simulation results match well with the analytical results in the air environment, i.e., the

second eigenmode resonance frequency ($f_2 = 6.3f_1$) and the third eigenmode resonance frequency ($f_3 = 17.5f_1$).

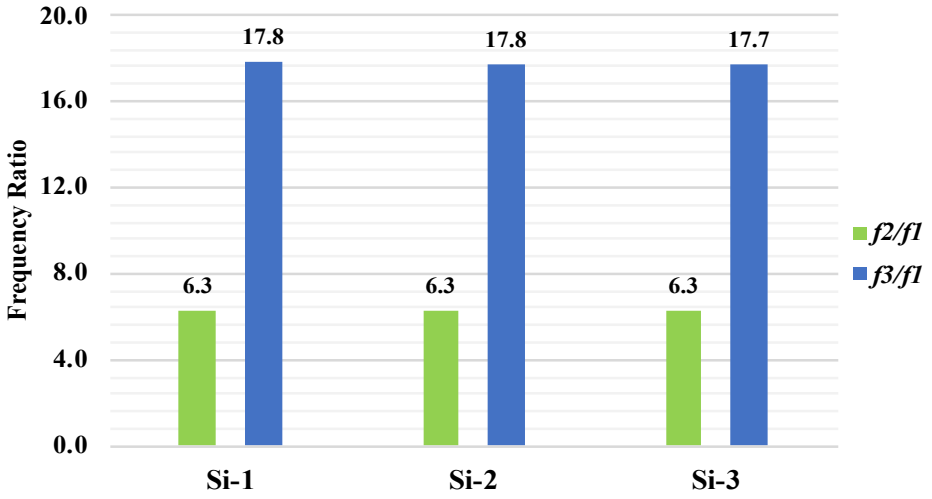

Figure 5.5. First three eigenmode frequency analysis of silicon cantilevers in air environment.

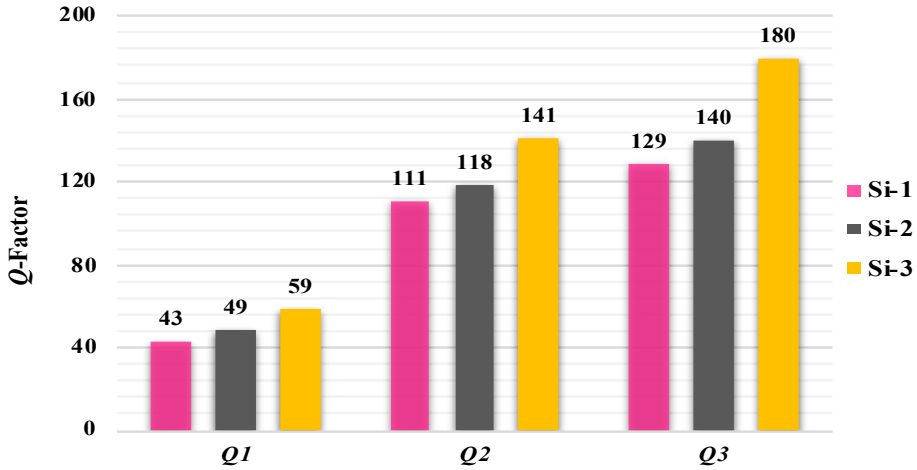

Figure 5.6. *Q*-factor analysis of silicon cantilevers in air environment.

Q-factor results are shown in Figure 5.6. Thickness plays an important role and *Q*-factor increases as the thickness of the cantilever increases.

5.2.1.2. Modified Cantilevers

This section explores the effect of adding a mass (AM-1,2) and cutting a hole (CH-1,2) (Figure 5.7) at either ends of rectangular cantilever (Si Cantilever 3), on

resonance frequencies and Q-factors. The diameters of these masses or holes are of 1 µm. An increase in all the three eigenmode Q-factors has been observed in Added-Mass cantilever beams while comparing to thicker rectangular cantilever with same dimensions. On the other hand, a reduction in first eigenmode Q-factor has seen in Cut-Holed cantilever geometry when compared to the thicker rectangular cantilever. In addition, as expected, a lower spring constant (k) of 0.6 N/m, is obtained for the cantilever geometry CH-1. Whereas, adding a mass at the fixed end, resulted in higher spring constant.

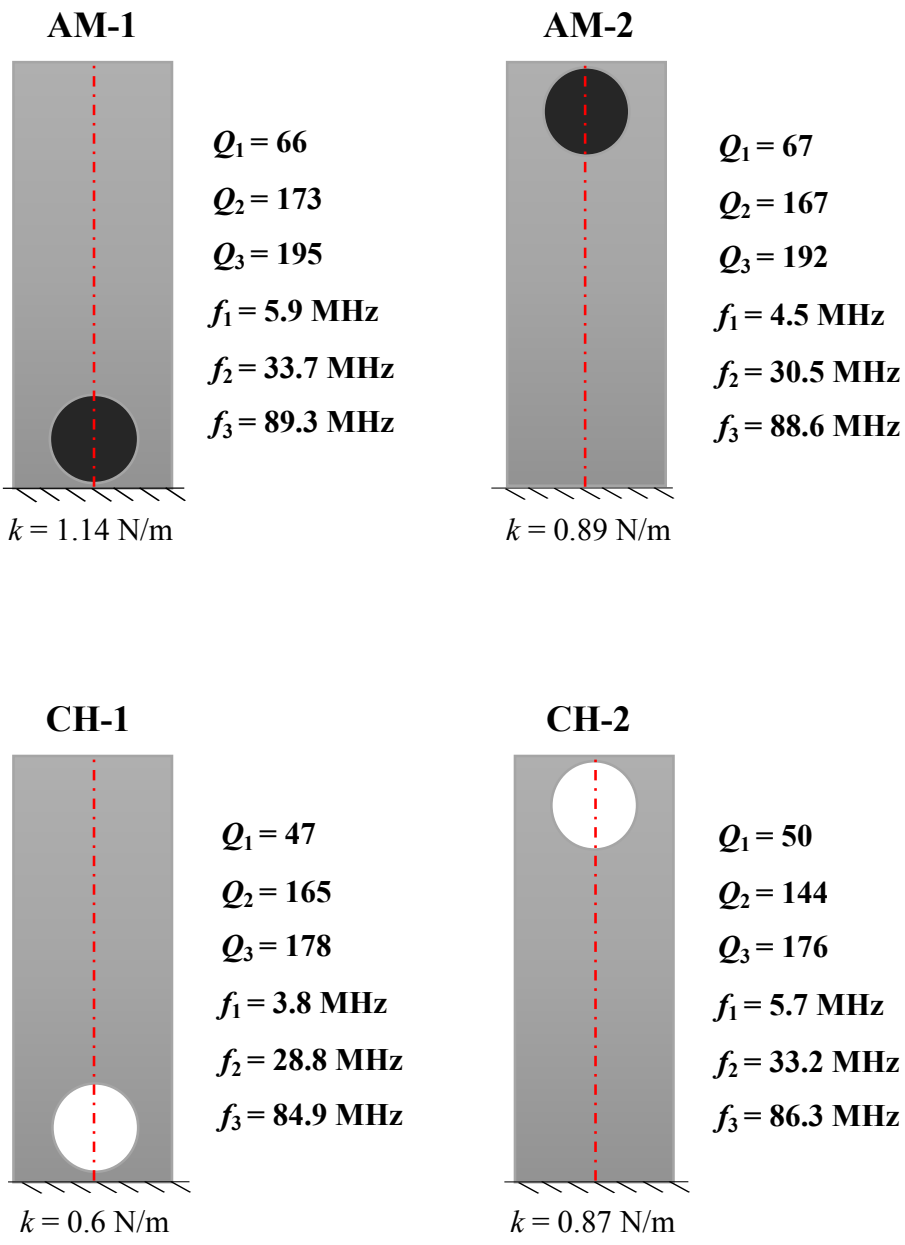

Figure 5.7. Effect of adding mass and cutting hole on resonance frequencies and Q-factors of thicker silicon rectangular cantilever in air environment.

Figure 5.8 and Figure 5.9 depict the comparison of resonance frequencies and *Q*-factors of four additional modified cantilevers with the original rectangular cantilever.

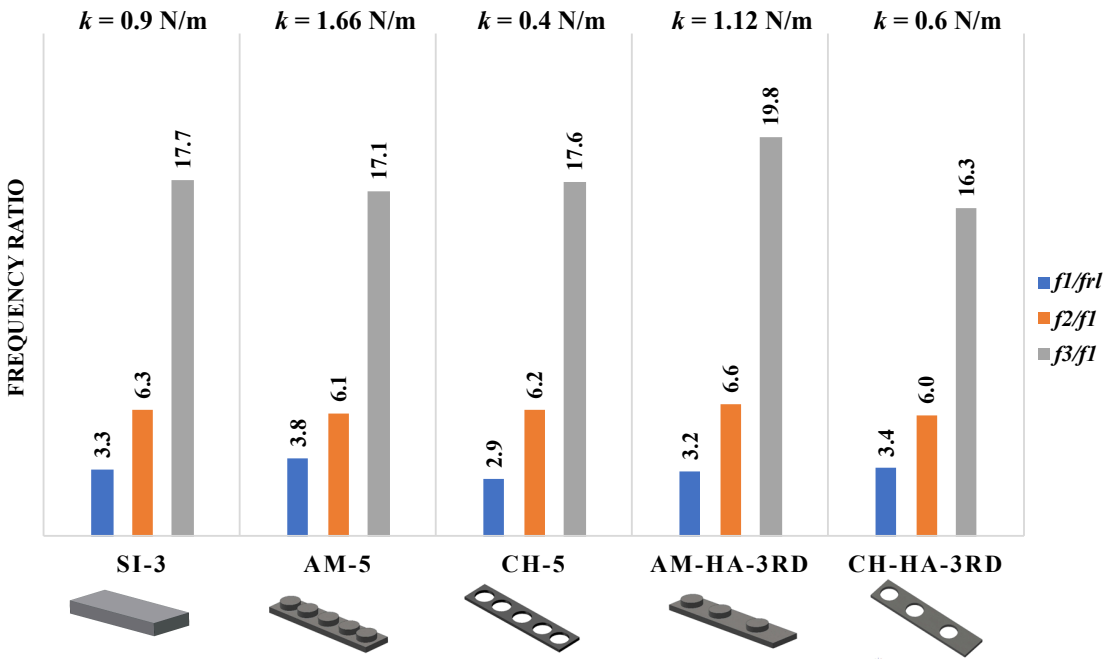

Figure 5.8. Resonance frequency analysis of modified Added-Mass and Cut-Holed silicon cantilever beams in air environment (resonance frequency in liquid: f_{rl} = 1.5 MHz).

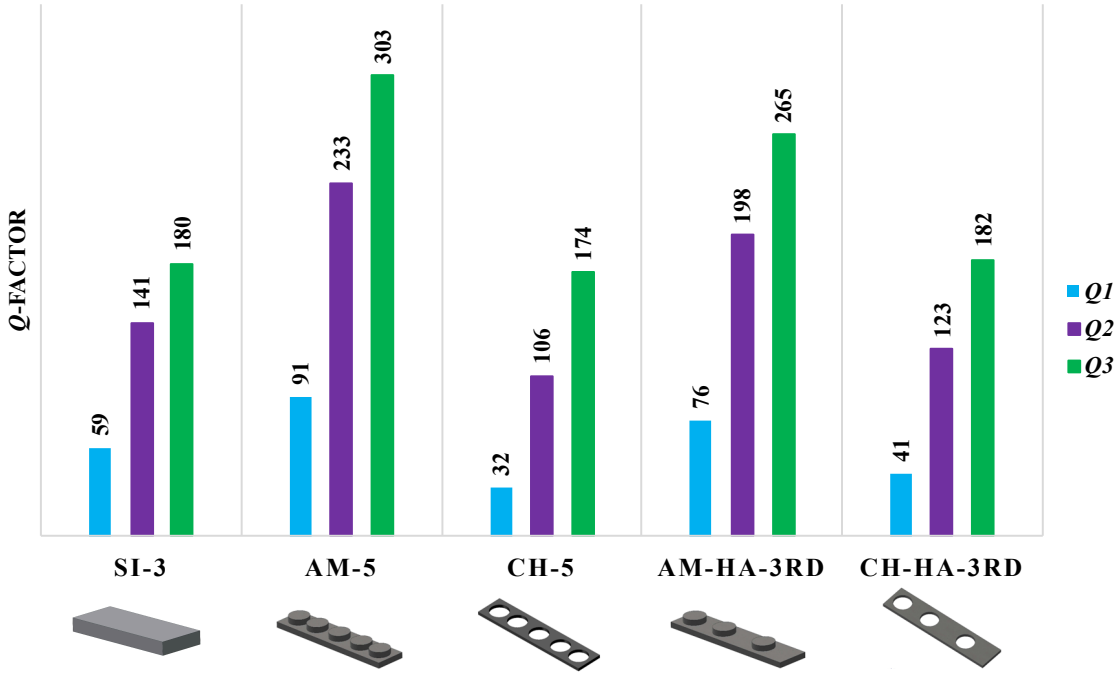

Figure 5.9. *Q*-factor analysis of modified Added-Mass and Cut-Holed silicon cantilevers in air environment.

AM-5 and CH-5 represents the adding five masses and cutting five holes at same lengths with 1 µm of diameter, to the regular rectangular cantilever beam. The added mass thickness is equal to the original cantilever thickness. While the remaining two cantilevers, marks the Added-Mass and Cut-Holes at high amplitude locations of the third eigenmode frequency. Adding a mass on five different locations increased the all three *Q*-factors significantly, while a reduction of *Q*-factors has been observed in the five Cut-Holed version of the cantilever. AM-HA-3RD cantilever shows higher *Q*-factors while comparing to Si-3, AM-1 and AM-2 cantilevers and lower than the AM-5 cantilever. Similarly, the CH-HA-3RD cantilever, shows lower *Q*-factors than Si-3, CH-1 and 2 cantilevers but higher than the CH-5 cantilever

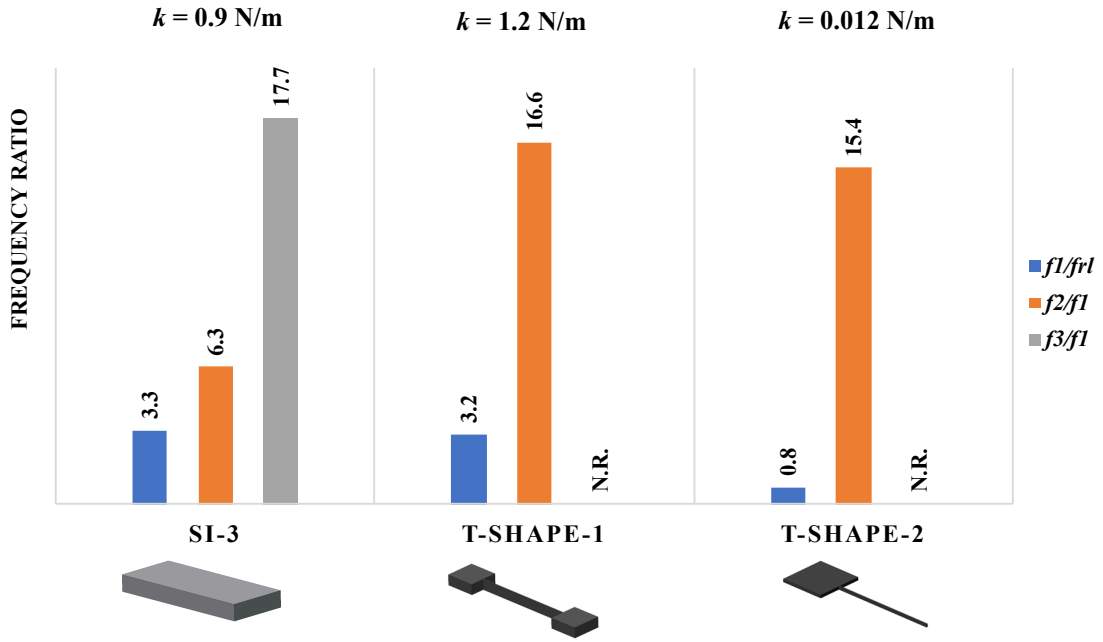

Figure 5.10. Resonance frequency analysis of modified T-Shaped silicon cantilevers in air environment (resonance frequency in liquid: f_{rl} = 1.5 MHz).

Additionally, two different T-Shaped geometries are also studied shown in Figure 5.10 and 5.11. The width at the fixed end of the T-Shape-2, and the middle of T-Shape-1 cantilever is 50 nm and the thickness is kept at 0.1 µm and 0.55 µm respectively. For the T-Shape-1, even though the spring constant (k) is 1.2 N/m, a considerable increment in the first eigenmode *Q*-factor has been observed, which is far greater than any other cantilever in the air environment. For T-Shape-2, a thickness of 0.1 µm results in very low spring constant (k) of 0.012 N/m and very low first eigenmode *Q*-factor of 9. Due to

the clamped-clamped behavior, the third eigenmode in both T-Shaped cantilever geometries have not been observed.

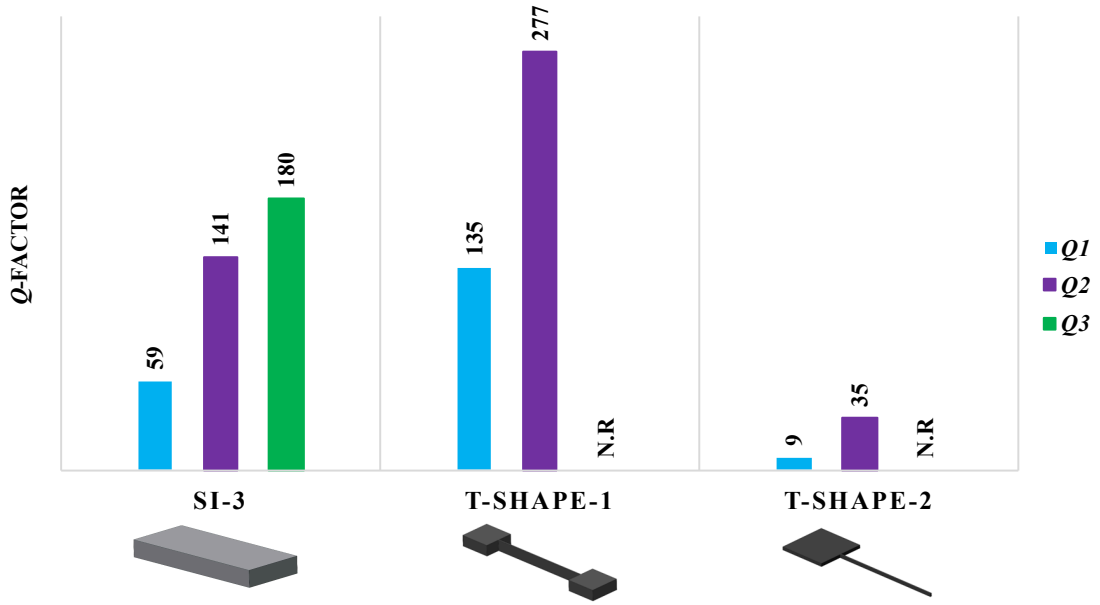

Figure 5.11. Q-factor analysis of T-Shaped silicon cantilevers in air environment. (N.R.: No Result)

5.2.2. Liquid Environment

The high-speed atomic force microscopy's success in evaluating dynamic process of proteins, enzymes in liquid environment suggests its importance in a variety of areas of nanotechnology. Therefore, evaluating the parameters like resonance frequency and Q-factor of rectangular cantilever beam in liquid plays a key role in HS-AFM imaging.

5.2.2.1. Rectangular Cantilevers

Similar to the air environment, the cantilever dimensions shown in Table 5.1, are used to maintain the first resonance frequency (f_r) of 1.5 MHz (± 10%) and a spring constant (k) of 0.9 N/m (± 10%) in liquid environment. As shown in Figure 5.12, a similar behavior for the resonance frequencies are observed for the thinner, moderate and thicker cantilevers. A higher ratio of resonance frequency is also recorded compared to the air environment results. This is due to the fact that mass loading effect on higher eigenmodes

is relatively small compared to first eigenmode in liquid environment (Norton and Karczub 2003).

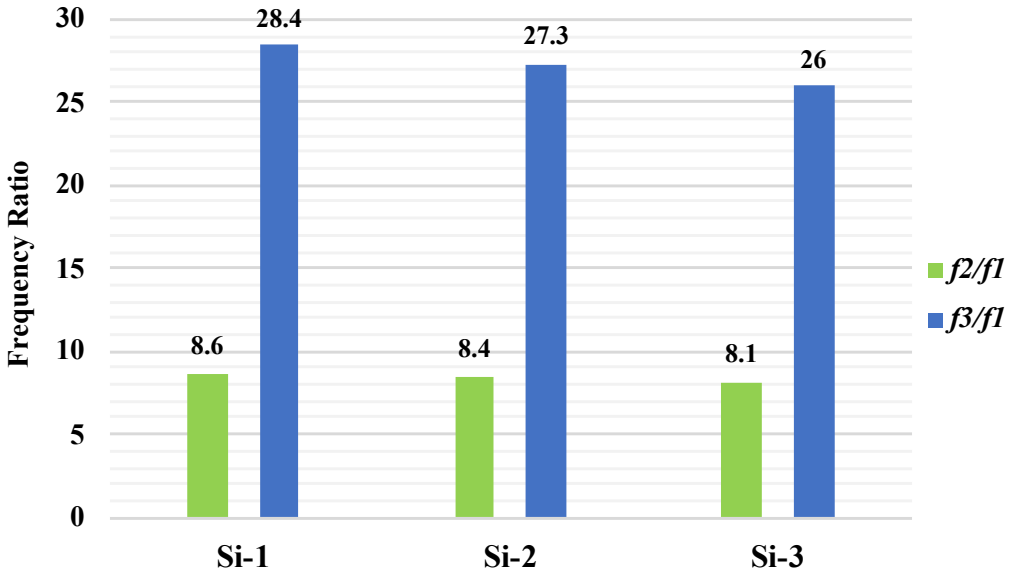

Figure 5.12. First three eigenmode frequency analysis of silicon cantilever beams in liquid environment.

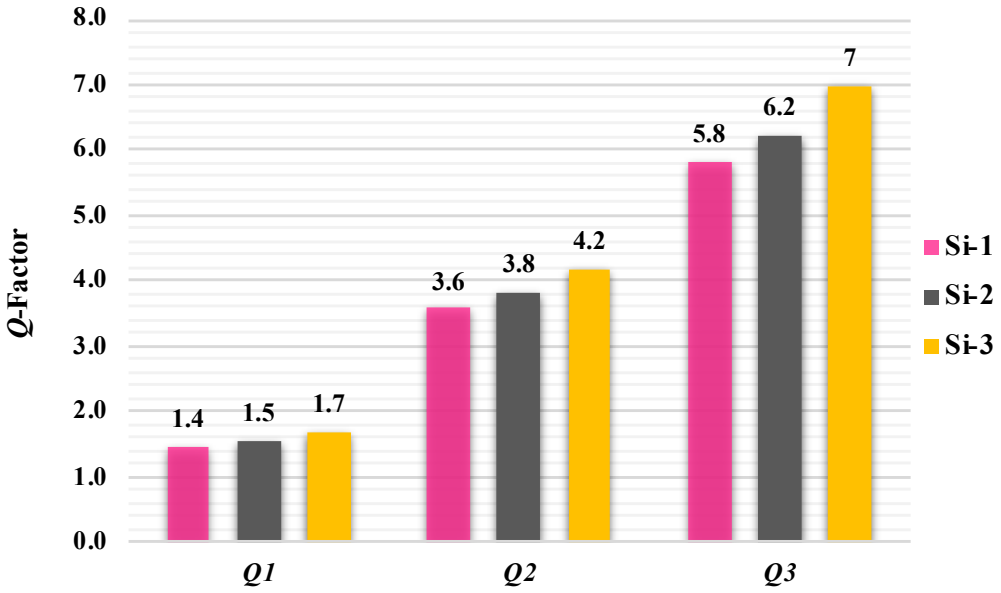

Figure 5.13. *Q*-factor analysis of silicon cantilevers in liquid environment.

Furthermore, due to high density of the water, the *Q*-factors are decreased significantly when compared to the air environment (Tröger and Reichling 2010). As shown in Figure 5.13, as the thickness of the rectangular cantilever beam increases, the *Q*-factor also increases. The *Q*-factor in the liquid environment is mostly affected by the

viscous damping of water. Due to this achieved low *Q*-factor, the force sensitivity is strongly diminished (Albrecht *et al.* 1991).

5.2.2.2. Modified Cantilevers

The resonance frequencies and *Q*-factors of certain modified cantilevers in the liquid environment is explored in this section. Table 5.2 shows the resonance frequency and *Q*-factor analysis of all the modified cantilevers in liquid environment. As discussed previously, due to the dominance of viscous damping in liquid environment, the cantilever beams show a similar *Q*-factor decrement behavior regardless of their geometry. T-Shape-1 and AM-5 cantilevers show a higher first eigenmode *Q*-factor of 1.8 than any other geometry.

5.3. High Frequency SU-8 Cantilevers

One popular method to increase the imaging rate in high-speed atomic force microscopy involves reducing the size significantly. Another approach is to change the material type. SU-8 material cantilevers with similar geometrical dimensions yield higher imaging bandwidth than traditional Silicon material cantilevers (Adams *et al.* 2015).

As the high-speed atomic force microscopy applications require very high imaging rate which closely relates to the cantilever properties. The approach to increase the imaging rate involves a significant reduction in size of cantilever (Walters *et al.* 1996) (Ando *et al.* 2001). Furthermore, to achieve high frequency, as seen in the traditional Silicon cantilever parameters studies above, the cantilever size shrinks to 0.11 μm in the thickness. To fabricate such a device is very challenging with current technology. Which also led researchers to change in detection methods (Li, Tang, and Roukes 2007) (Antognozzi *et al.* 2008) (Sanii and Ashby 2010). To overcome such shortcomings, different materials has been explored. Recently, SU-8 (a Polymer material) is studied for high-speed AFM application (Adams *et al.* 2015). Similar to the high frequency Silicon cantilevers, a fixed first resonance frequency (f_r) of 1.5 MHz (± 10 %) in liquid and 5 MHz (± 10 %) in air environments, and a spring constant (k) of 0.9 N/m (± 10 %) is maintained while choosing the rectangular cantilever dimensions.

Table 5.2. Resonance frequency and *Q*-factor analysis of modified cantilevers in liquid environment. (N.R.: No Result)

Cantilever Type	f_1 (MHz)	f_2 (MHz)	f_3 (MHz)	Q_1	Q_2	Q_3
AM-1 	2.1	15.4	46	1.6	3.9	6.5
AM-2 	1.7	14.3	45.6	1.5	3.8	6.7
CH-1 	1.2	13.1	44.2	1.3	3.5	5.6
CH-2 	1.8	15.5	45.1	1.1	2.7	4.8
AM-5 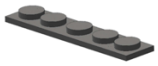	2.5	18.5	57.1	1.8	4.5	7.8
CH-5 	1.1	13.1	43.8	0.8	1.7	2.9
AM-HA-3RD 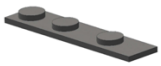	1.9	15.9	54.9	1.6	4.1	7.2
CH-HA-3RD 	1.4	14.7	46.7	0.9	2.14	3.3
T-Shape-1 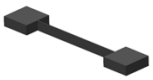	2.7	N.R.	N.R.	1.8	N.R.	N.R.
T-Shape-2 	0.12	5.2	N.R.	0.3	0.8	N.R.

5.3.1. Air Environment

For the fixed first eigenmode resonance frequency and spring constant, the dimensions given in Table 5.3 are selected. When compared to the Silicon cantilever dimensions, there is a significant difference in thickness due to lower Young's Modulus of SU-8. A spring constant of 0.9 N/m (± 10%) for these rectangular cantilever dimensions are measured.

Table 5.3. SU-8 rectangular cantilever dimensions.

Type	Length (µm)	Width (µm)	Thickness (µm)
SU-8 Cantilever 1	5.7	1.8	0.45
SU-8 Cantilever 2	6.3	1.3	0.55
SU-8 Cantilever 3	6.9	1	0.65

We find similar results for the thinner, moderate and thicker SU-8 cantilevers in the air environment. The first eigenmode resonance frequency is found to be approximately 3.7 MHz and the *Q*-factor is around 11 for all of the cantilevers. SU-8's viscoelastic properties certainly help in decreasing of *Q*-factor even in the air environment. The levels of *Q*-factors are highly suppressed compared to the Silicon counterparts in the air environment.

5.3.2. Liquid Environment

Evaluating parameters like resonance frequency, *Q*-factor and spring constant of SU-8 cantilevers in high damping environment like liquid is a key study to further use in high-speed atomic force microscopy applications.

The first eigenmode resonance frequency and *Q*-factor for these cantilevers are again found to be very close to each other like in air environment. We find that the first eigenmode resonance frequency is close to 1.5 MHz and the *Q*-factor is about 1.3 for all of the cantilevers. The *Q*-factors are suppressed further in the high damping liquid environment which suggests the combined effect of liquid damping and material's viscoelastic damping.

5.3.3. The effect of Viscoelasticity

The viscoelastic behavior of SU-8 material is captured through a complex Young's Modulus defined as

$$E = E' + iE'' \tag{5.1}$$

where, E' is the storage modulus and E'' is the loss modulus.

The complex nature of SU-8's Young's modulus influences the *Q*-factor. Therefore, it appears as an additional factor (eq. 5.2) with other damping losses affecting the *Q*-factor (Adams *et al.* 2015).

$$Q^{-1} = {Q_{visc}}^{-1} + \frac{E''}{2E'} \tag{5.2}$$

A theoretical and experimental analysis of a SU-8 rectangular cantilever's first eigenmode frequency and *Q*-factor with the length of 25 µm, width of 10 µm and thickness of 2.5 µm in air environment was made by Adams *et al.* (2015). For the analysis, a storage modulus (E') of 4 GPa and a loss modulus (E'') of 0.15 GPa was used. A first eigenmode frequency of 1.69 MHz and *Q*-factor of 33 was observed by Adams *et al.* (2015).

To match the above results, a SU-8 rectangular cantilever with a slight increase in thickness to 3.4 µm, with a viscosity of 5 Pa.s and a shear modulus of 1.3 GPa are used in this study.

To analyze how the viscosity of the material affects the *Q*-factor, simulations are performed at various viscosity levels. Figure 5.14 shows the first eigenmode *Q*-factor analysis of the rectangular SU-8 cantilever beam. A continuous decline in the *Q*-factor is observed, when the viscosity level changed from 1 to 100 Pa.s. However, at higher viscosity around 1 to 10 kPa.s, the *Q*-factor remains constant. In addition, the *Q*-factor remains constant at ~450 for lower values of viscosity, i.e., 0.01 to 0.1 Pa.s. The analysis shows a greater deal into how the *Q*-factor of a rectangular cantilever can be easily modified by controlling the viscosity of the material.

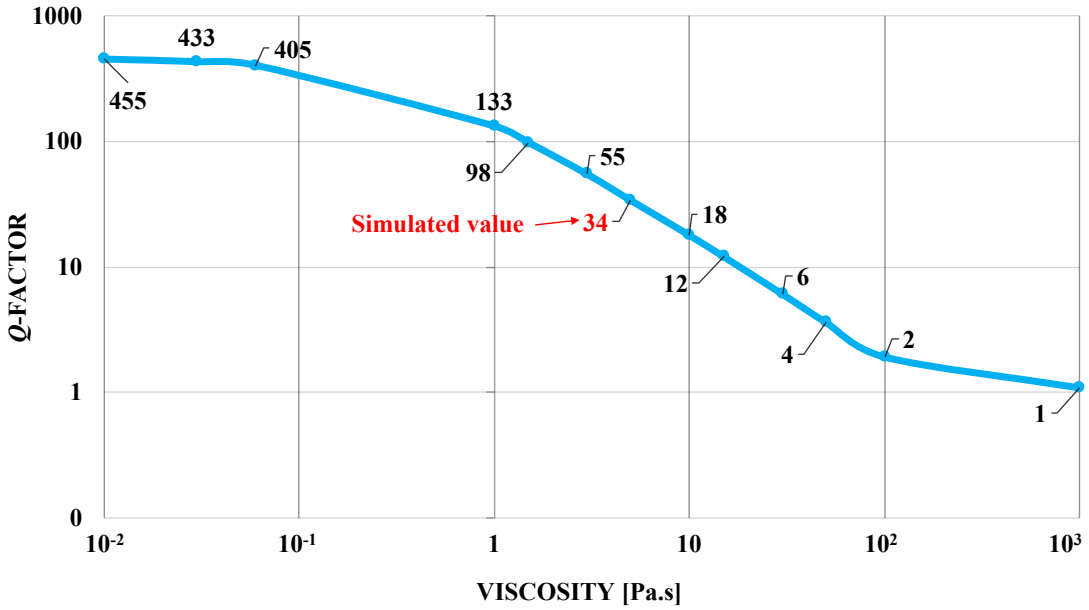

Figure 5.14. First eigenmode *Q*-factor analysis at different viscosity level of SU-8 rectangular cantilever in air environment.

CHAPTER 6

CONCLUSIONS AND PERSPECTIVES

The conventional high-speed atomic force microscopy uses the first flexural eigenmode for the operation. In another method of HS-AFM operation, higher eigenmodes are used as well (Balantekin 2015). Therefore, this work revolves around the Q-factor and resonance frequency (f_r) analysis of first three flexural eigenmodes of small high frequency cantilevers in both air and liquid environments. Numerous small rectangular and modified cantilevers are analyzed for high frequency operations. First to validate the simulation environment, various comparisons with prior studies in the literature are made. These prior study comparisons systematically evaluate effects of pressure, nature of surrounding environment and presence of nearby surface (squeeze film effect) on the Q-factors and resonance frequency (f_r) of cantilevers. We find a good agreement between our results and the ones in the literature.

For Silicon rectangular cantilevers in the air environment, for the same resonance frequency and spring constant, the Q-factor increases with the increase in thickness of the geometry (or decrease in surface area). Adding a mass and cutting a hole at either ends of the thicker rectangular cantilever showed manipulation in Q-factors. For Added-Mass geometries, an approximate 15% increase in first eigenmode Q-factor has been obtained. On the other hand, Cut-Holed geometries decreases the Q-factor by up-to 20%.

For deeper understanding of the effect of geometries on Q-factors, more sophisticated geometries are designed and analyzed. The Q-factor can be easily manipulated by increasing mass or cutting holes at certain locations on the rectangular cantilever. A significant increase of 55% in Q-factor is shown by AM-5 cantilever. In addition, a 0.2 μm thick cantilever is analyzed and compared with AM-5 cantilever, which results in lower Q-factor and higher spring constant than the AM-5 cantilever. Thus, adding a mass on specific locations, certainly helps in increasing the Q-factor. On the other hand, the Cut-Holed version with similar five-hole pattern show a 55% decrement in Q-factor.

Furthermore, two different T-Shape geometries are investigated. To achieve higher first eigenmode Q-factor, the thickness of the cantilever is increased to 0.55 μm. However, to keep the spring constant low, the width of the connecting part of T-Shape-1

is kept at bare 50 nm and it results in an increase of Q-factor by 130% when compared to the Si-3 cantilever. On the other hand, the T-Shape-2 with 0.1 μm of thickness resulted in 4 times less first eigenmode frequency and the lowest first eigenmode Q-factor with a decrement of 85%. Moreover, due to the clamped-clamped behavior at higher eigenmode frequencies, the third eigenmode is not observed in both shapes.

In liquid environment, due to viscous damping of water, a significant drop in Q-factors is measured and a notable increment in the f_3/f_1 ratio is identified. Similar to air environment counterparts, thicker rectangular cantilever geometry provides higher Q-factors. Furthermore, the modified cantilever shows the similar behavior in Q-factors. Similar to its counterpart in air environment the AM-5 cantilever shows higher Q-factor. T-Shape-1 and AM-5 show the highest Q-factor among all the cantilever geometries. Whereas, the T-Shape-2 exhibits the lowest Q-factor with lowest resonance frequency of 0.12 MHz.

A Polymer material SU-8 is also investigated later in the study. The thickness of cantilevers is increased by approximately 4 times because of SU-8's low Young's Modulus. Due to the dominance of viscoelasticity property of SU-8 material, the Q-factor analysis in air and liquid environment exhibits lower Q-factors than the Silicon cantilevers regardless of the geometry. Additionally, this work also exhibits the importance of viscoelasticity of material in manipulating the Q-factors.

This work demonstrates a great opportunity to choose different cantilever geometries and materials for high-speed atomic force microscopy applications in air and liquid environments. Any future work could use the focus ion beam system to add or remove the mass from cantilever geometries discussed in this study. In this way, experimental validation of the simulation results can be done. The implications of obtained results on various multifrequency imaging methods can be explored on different simulation platforms.

REFERENCES

Adams, Jonathan D., Blake W. Erickson, Jonas Grossenbacher, Juergen Brugger, Adrian Nievergelt, and Georg E. Fantner. 2015. "Harnessing the damping properties of materials for high-speed atomic force microscopy." *Nature Nanotechnology* 11:147. doi: 10.1038/nnano.2015.254 https://www.nature.com/articles/nnano.2015.254#supplementary-information.

Akamine, S., R. C. Barrett, and C. F. Quate. 1990. "Improved atomic force microscope images using microcantilevers with sharp tips." *Applied Physics Letters* 57 (3):316-318. doi: 10.1063/1.103677.

Albrecht, T. R., P. Grütter, D. Horne, and D. Rugar. 1991. "Frequency modulation detection using high-Q cantilevers for enhanced force microscope sensitivity." *Journal of Applied Physics* 69 (2):668-673. doi: 10.1063/1.347347.

Ando, T. 2012. "High-speed atomic force microscopy coming of age." *Nanotechnology* 23 (6):062001. doi: 10.1088/0957-4484/23/6/062001.

Ando, Toshio, Noriyuki Kodera, Eisuke Takai, Daisuke Maruyama, Kiwamu Saito, and Akitoshi Toda. 2001. "A high-speed atomic force microscope for studying biological macromolecules." *Proceedings of the National Academy of Sciences* 98 (22):12468-12472.

Andrews, M., I. Harris, and G. Turner. 1993. "A comparison of squeeze-film theory with measurements on a microstructure." *Sensors and Actuators A: Physical* 36 (1):79-87. doi: https://doi.org/10.1016/0924-4247(93)80144-6.

Antognozzi, M., A. Ulcinas, L. Picco, S. H. Simpson, P. J. Heard, M. D. Szczelkun, B. Brenner, and M. J. Miles. 2008. "A new detection system for extremely small vertically mounted cantilevers." *Nanotechnology* 19 (38):384002.

Balantekin, M. 2015. "High-speed dynamic atomic force microscopy by using a Q-controlled cantilever eigenmode as an actuator." *Ultramicroscopy* 149:45-50. doi: https://doi.org/10.1016/j.ultramic.2014.11.016.

Bao, Minhang, and Heng Yang. 2007. "Squeeze film air damping in MEMS." *Sensors and Actuators A: Physical* 136 (1):3-27.

Binnig, G., C. F. Quate, and C. Gerber. 1986. "Atomic force microscope." *Phys Rev Lett* 56 (9):930-933. doi: 10.1103/PhysRevLett.56.930.

Binnig, G., and H. Rohrer. 1983. "Scanning tunneling microscopy." *Surface Science* 126 (1):236-244. doi: https://doi.org/10.1016/0039-6028(83)90716-1.

Blom, F. R., S. Bouwstra, M. Elwenspoek, and J. H. J. Fluitman. 1992. "Dependence of the quality factor of micromachined silicon beam resonators on pressure and geometry." *Journal of Vacuum Science & Technology B: Microelectronics and Nanometer Structures Processing, Measurement, and Phenomena* 10 (1):19-26. doi: 10.1116/1.586300.

Braunsmann, Christoph, and Tilman E. Schäffer. 2010. "High-speed atomic force microscopy for large scan sizes using small cantilevers." *Nanotechnology* 21 (22):225705.

Calabri, L., N. Pugno, C. Menozzi, and Sergio Valeri. 2008. "AFM nanoindentation: tip shape and tip radius of curvature effect on the hardness measurement." *Journal of Physics: Condensed Matter* 20 (47):474208.

Colom, Adai, Ignacio Casuso, Thomas Boudier, and Simon Scheuring. 2012. "High-Speed Atomic Force Microscopy: Cooperative Adhesion and Dynamic Equilibrium of Junctional Microdomain Membrane Proteins." *Journal of Molecular Biology* 423 (2):249-256.

Cullen, P., K. Cox, M. Bin Subhan, L. M. Picco, Oliver D. Payton, D. Buckley, S. Hodge, N. Skipper, V. Tileli, and C. Howard. 2016. "Ionic Solutions of 2-dimensional materials." *Chemistry* 9 (3):244-249.

Fadel, L., F. Lochon, I. Dufour, and O. Français. 2004. "Chemical sensing: millimeter size resonant microcantilever performance." *Journal of Micromechanics and Microengineering* 14 (9):S23.

Hashimoto, Manami, Noriyuki Kodera, Yasuo Tsunaka, Masayuki Oda, Mitsuru Tanimoto, Toshio Ando, Kosuke Morikawa, and Shin-ichi Tate. 2013. "Phosphorylation-Coupled Intramolecular Dynamics of Unstructured Regions in Chromatin Remodeler FACT." *Biophysical Journal* 104 (10):2222-2234. doi: https://doi.org/10.1016/j.bpj.2013.04.007.

Igarashi, Kiyohiko, Takayuki Uchihashi, Anu Koivula, Masahisa Wada, Satoshi Kimura, Tetsuaki Okamoto, Merja Penttilä, Toshio Ando, and Masahiro Samejima. 2011. "Traffic Jams Reduce Hydrolytic Efficiency of Cellulase on Cellulose Surface." *Science* 333 (6047):1279.

Itani, Toshiro, and Julius Joseph Santillan. 2010. "In situ characterization of photoresist dissolution." *Applied physics express* 3 (6):061601.

Kodera, N., D. Yamamoto, R. Ishikawa, and T. Ando. 2010. "Video imaging of walking myosin V by high-speed atomic force microscopy." *Nature* 468 (7320):72-6. doi: 10.1038/nature09450.

Laferrere, Alice, Robert Burrows, Carol Glover, Ronald Nuuchin Clark, Oliver Payton, Loren Picco, Stacy Moore, and Geraint Williams. 2017. "In situ imaging of corrosion processes in nuclear fuel cladding." *Corrosion Engineering, Science and Technology* 52 (8):596-604. doi: 10.1080/1478422X.2017.1344038.

Li, Mo, Hong X. Tang, and Michael L. Roukes. 2007. "Ultra-sensitive NEMS-based cantilevers for sensing, scanned probe and very high-frequency applications." *Nature nanotechnology* 2 (2):114.

Martin, Y., C. C. Williams, and H. K. Wickramasinghe. 1987. "Atomic force microscope–force mapping and profiling on a sub 100-Å scale." *Journal of Applied Physics* 61 (10):4723-4729. doi: 10.1063/1.338807.

Mertens, Johann, Eric Finot, Thomas Thundat, Arnaud Fabre, Marie-Hélène Nadal, Vincent Eyraud, and Eric Bourillot. 2003. "Effects of temperature and pressure on microcantilever resonance response." *Ultramicroscopy* 97 (1):119-126. doi: https://doi.org/10.1016/S0304-3991(03)00036-6.

Meyer, Gerhard, and Nabil M. Amer. 1988. "Novel optical approach to atomic force microscopy." *Applied Physics Letters* 53 (12):1045-1047. doi: 10.1063/1.100061.

Miyagi, Atsushi, Toshio Ando, and Yuri L. Lyubchenko. 2011. "Dynamics of Nucleosomes Assessed with Time-Lapse High-Speed Atomic Force Microscopy." *Biochemistry* 50 (37):7901-7908. doi: 10.1021/bi200946z.

Newell, William E. 1968. "Miniaturization of Tuning Forks." *Science* 161 (3848):1320.

Nievergelt, Adrian P., Jonathan D. Adams, Pascal D. Odermatt, and Georg E. Fantner. 2014. "High-frequency multimodal atomic force microscopy." *Beilstein journal of nanotechnology* 5:2459.

Noi, Kentaro, Daisuke Yamamoto, Shingo Nishikori, Ken-ichi Arita-Morioka, Takayuki Kato, Toshio Ando, and Teru Ogura. 2013. "High-Speed Atomic Force Microscopic Observation of ATP-Dependent Rotation of the AAA+ Chaperone p97." *Structure* 21 (11):1992-2002.

Norton, Michael Peter, and Denis G. Karczub. 2003. *Fundamentals of noise and vibration analysis for engineers*: Cambridge university press.

Payton, O. D., L. Picco, and T. B. Scott. 2016. "High-speed atomic force microscopy for materials science." *International Materials Reviews* 61 (8):473-494.

Payton, O. D., L. Picco, T. Scott, A. Raman, J. E. Sader, J. Killgore, and D. C. Hurley. 2016. "Development of a high-speed contact resonance force microscope." *Submitted to IOP Nanotechnology*.

Pyne, Alice, Will Marks, Loren M. Picco, Peter G. Dunton, Arturas Ulcinas, Michele E. Barbour, Siân B. Jones, James Gimzewski, and Mervyn J. Miles. 2009. "High-speed atomic force microscopy of dental enamel dissolution in citric acid." *Archives of histology and cytology* 72 (4+ 5):209-215.

Qiu, Huacheng. 2014. "Dynamics of oscillating piezoelectric micro resonators: Hydrodynamic loading effect and intrinsic damping."PhD Dissertation, Physik und Mechatronik, Universität des Saarlandes.

Sandberg, R., Kristian Mølhave, Anja Boisen, and W. Svendsen. 2005. "Effect of gold coating on the Q-factor of a resonant cantilever." *Journal of Micromechanics and Microengineering* 15 (12):2249.

Sanii, Babak, and Paul D. Ashby. 2010. "High sensitivity deflection detection of nanowires." *Physical review letters* 104 (14):147203.

Sekaric, L., D. W. Carr, S. Evoy, J. M. Parpia, and H. G. Craighead. 2002. "Nanomechanical resonant structures in silicon nitride: fabrication, operation and dissipation issues." *Sensors and Actuators A: Physical* 101 (1-2):215-219.

Seong, Myunghoon, Suhas Somnath, Hoe Joon Kim, and William P. King. 2014. "Parallel nanoimaging using an array of 30 heated microcantilevers." *RSC Advances* 4 (47):24747-24754.

Shibata, Mikihiro, Takayuki Uchihashi, Hayato Yamashita, Hideki Kandori, and Toshio Ando. 2011. "Structural Changes in Bacteriorhodopsin in Response to Alternate Illumination Observed by High-Speed Atomic Force Microscopy." *Angewandte Chemie International Edition* 50 (19):4410-4413. doi: 10.1002/anie.201007544.

Suzuki, Aussie, Tetsuya Hori, Tatsuya Nishino, Jiro Usukura, Atsushi Miyagi, Kosuke Morikawa, and Tatsuo Fukagawa. 2011. "Spindle microtubules generate tension-dependent changes in the distribution of inner kinetochore proteins." *The Journal of Cell Biology* 193 (1):125.

Suzuki, Yasumasa, Hirotoshi Enoki, and Etsuo Akiba. 2004. "Investigation of influence of gas atmosphere and pressure upon non-contact atomic force microscopy." *Ultramicroscopy* 99 (4):221-226.

Tortonese, M., R. C. Barrett, and C. F. Quate. 1993. "Atomic resolution with an atomic force microscope using piezoresistive detection." *Applied Physics Letters* 62 (8):834-836. doi: 10.1063/1.108593.

Tröger, L., and M. Reichling. 2010. "Quantification of antagonistic optomechanical forces in an interferometric detection system for dynamic force microscopy." *Applied Physics Letters* 97 (21):213105. doi: 10.1063/1.3509412.

Uchihashi, Takayuki, Ryota Iino, Toshio Ando, and Hiroyuki Noji. 2011. "High-Speed Atomic Force Microscopy Reveals Rotary Catalysis of Rotorless F_1-ATPase." *Science* 333 (6043):755-758. doi: 10.1126/science.1205510.

Uchihashi, Takayuki, Noriyuki Kodera, and Toshio Ando. 2012. "Guide to video recording of structure dynamics and dynamic processes of proteins by high-speed atomic force microscopy." *nature protocols* 7 (6):1193.

Walters, D. A., J. P. Cleveland, N. H. Thomson, P. K. Hansma, M. A. Wendman, G. Gurley, and V. Elings. 1996. "Short cantilevers for atomic force microscopy." *Review of Scientific Instruments* 67 (10):3583-3590. doi: 10.1063/1.1147177.

Wolter, O., Th Bayer, and J. Greschner. 1991. "Micromachined silicon sensors for scanning force microscopy." *Journal of Vacuum Science & Technology B: Microelectronics and Nanometer Structures Processing, Measurement, and Phenomena* 9 (2):1353-1357. doi: 10.1116/1.585195.

Yamashita, Hayato, Azuma Taoka, Takayuki Uchihashi, Tomoya Asano, Toshio Ando, and Yoshihiro Fukumori. 2012. "Single-molecule imaging on living bacterial cell surface by high-speed AFM." *Journal of molecular biology* 422 (2):300-309.

Yamashita, Hayato, Kislon Voïtchovsky, Takayuki Uchihashi, Sonia Antoranz Contera, John F. Ryan, and Toshio Ando. 2009. "Dynamics of bacteriorhodopsin 2D crystal observed by high-speed atomic force microscopy." *Journal of Structural Biology* 167 (2):153-158. doi: https://doi.org/10.1016/j.jsb.2009.04.011.

Yilmaz, Neval, Taro Yamada, Peter Greimel, Takayuki Uchihashi, Toshio Ando, and Toshihide Kobayashi. 2013. "Real-Time Visualization of Assembling of a Sphingomyelin-Specific Toxin on Planar Lipid Membranes." *Biophysical Journal* 105 (6):1397-1405. doi: https://doi.org/10.1016/j.bpj.2013.07.052.